Information and entanglement measures applied to the analysis of complexity in doubly excited states of helium

J. P. Restrepo Cuartas and J. L. Sanz-Vicario*

Grupo de Física Atómica y Molecular, Instituto de Física, Universidad de Antioquia, Medellín, Colombia

(Received 21 October 2014; revised manuscript received 26 February 2015; published 1 May 2015)

Shannon entropy and Fisher information calculated from one-particle density distributions and von Neumann and linear entropies (the latter two as measures of entanglement) computed from the reduced one-particle density matrix are analyzed for the $^{1,3}S^e$, $^{1,3}P^o$, and $^{1,3}D^e$ Rydberg series of He doubly excited states below the second ionization threshold. In contrast with the Shannon entropy, we find that both the Fisher information and entanglement measures are able to discriminate low-energy resonances pertaining to different ${}_2(K,T)^A_{n_2}$ series according to the Herrick-Sinanoğlu-Lin classification. Contrary to bound states, which show a clear and unique asymptotic value for both Fisher information and entanglement measures in their Rydberg series $1s n\ell$ for $n \to \infty$ (which implies a loss of spatial entanglement), the variety of behaviors and asymptotic values of entanglement above the noninteracting limit value in the Rydberg series of doubly excited states ${}_2(K,T)^A_{n_2}$ indicates a signature of the intrinsic complexity and remnant entanglement in these high-lying resonances even with infinite excitation $n_2 \to \infty$, for which all known attempts of resonance classifications fail in helium.

DOI: 10.1103/PhysRevA.91.052301 PACS number(s): 03.67.Mn, 03.65.Ud, 31.15.vj

I. INTRODUCTION

The electronic density $\rho(\mathbf{r})$ in atoms, molecules, and solids is, in general, a distribution that can be observed experimentally, containing spatial information projected from the total quantum wave function. These density distributions in atoms can be thought as probability distributions subject to the scrutiny of the analytical methods in information theory. For example, Shannon entropy, Fisher information, disequilibrium, complexity measures analyzed in the Fisher-Shannon plane, and divergence measures between different densities (such as the Jensen-Shannon or Fisher divergences) have been used to study the information behavior of some atomic properties (see Refs. [1–5]). The Shannon entropy measures the spread, extent, and compactness of the spatial density in global way. Strictly speaking, it is not an observable of the system since there is no Hermitian operator associated with it in the Hilbert space, but it acts as a *theoretic-information* measure of the spatial uncertainty in the localization of the electrons in the system. In this work we will be concerned with the two-electron helium atom. In this respect, for instance, the Shannon entropy has already been studied in the two-electron Hooke's atom [6] and in confined simple atoms [1], as well as the scaling properties of the Shannon entropy near the ionization threshold for a two-electron atom [7]. The Fisher information provides instead a local analysis of the density distribution through its gradient content and it has been the subject of several studies in one-particle quantum systems [8,9] and two-electron artificial atoms [2], but to our knowledge, there is no previous study on Fisher information as applied to the helium atom.

Another tool to analyze states in quantum systems is through entanglement measures, such as von Neumann and linear entropies of entanglement [10–13]. Needless to say that entanglement is one of the most crucial properties of multipartite systems in quantum theory that brings essential inseparability and nonclassical correlations among their constituents, and it is subject to a continuous debate on its nature and potential applications. Previous studies have focused their attention on analyzing entanglement entropies of bound levels in artificial model atoms [14–22]. More recently, these studies have been extended to realistic two-electron atoms considered as bipartite entangled systems, although restricted to the analysis of the ground state and low-lying singly excited states [19,23–33].

The genuine manifestation of entanglement in a fermionic system is connected to the consideration of the Slater-Schmidt rank of the many-particle wave function as well as the value of the von Neumann entropy of the one-particle reduced density matrix [11,34,35]. Many electron atomic states expressed as a multiconfigurational wave function contain expansions in terms of many Slater determinants built with a set of orthogonal orbitals. Generally, this implies Slater ranks greater than 1 and, consequently, they are firm candidates to exhibit entanglement among their electrons. The von Neumann and linear entropies for any entangled state should be larger than the respective statistical minimum entropy corresponding to the simpler wave function with Slater rank unity (independent-particle-model states or Hartree-Fock states). There are many open questions on the proper choice of a measure to quantify the amount of entanglement in general fermionic systems, but it is widely accepted that for a two-electron system described as a pure state, the entanglement defined in terms of the von Neumann entropy of the reduced density matrix is definitely a good quantifier for entanglement (see, for example, Refs. [11,25,34,35]). On theoretical grounds, the greater the value of the von Neumann entropy, the larger the entanglement and the ensuing correlation among particles, although practical examples with excited states show the opposite, which requires new interpretations [19,30]. The use of the linear entropy is also firmly established [11,36]. Both linear and von Neumann entropies were calculated and compared for the Hooke's atom, for different confining harmonic potentials, to find that the

*Corresponding author: jose.sanz@udea.edu.co; present address: Departamento de Química, Módulo 13, Universidad Autónoma de Madrid, 28049 Madrid, Spain.

linear entropy (properly scaled) and the von Neumann entropy coincide qualitatively [25]. In Refs. [24,37] the behavior of the von Neumann entropy at the critical threshold point where a bound state in He becomes unbound by varying a parameter was studied. However, their study was restricted to the lowest singlet and triplet states with $L = 0$ and using a spherical helium model, where $1/r_{12}$ is replaced by $1/r_>$. Entanglement in emerging resonances of two-electron quantum dots using a model of two electrons confined in a spherical well of varying radius has also been recently reported [16]. Leaving apart two-electron model systems, specific studies for entanglement in realistic He atoms have also been carried out [19,29,30,32,33,38]. In these latter works entanglement measures have been analyzed only for some bound states of He. In Refs. [19,29] and Ref. [33] the authors compute He atom using Kinoshita-type and Hylleras-type explicitly correlated wave functions, respectively. In Refs. [30] and [32] the authors use the configuration interaction (CI) method, using orthogonal Slater-type functions and hydrogen-like orbitals in terms of the B-splines basis, respectively, to build uncorrelated two-electron configurations. The latter CI methods are similar to our method of solution.

The purpose in this work is to explore doubly excited states (DES) of helium atom as compared to singly excited states from the perspective of the topological information present in their spatial one-particle density as well as from their entanglement content measured with von Neumann and linear entropies (using the reduced one-particle density matrix). According to the Fano theory DES are no longer bound states since the electron correlation mixes the bound configurations of these states with the unbound electron configurations corresponding to the continuum of the same energy [39,40]. This means that these superexcited states lying in the continuum above one or more ionization thresholds contain both bound-like and scattering-like properties in their structure. The bound-like part of these resonances implies a strong localization of their density in regions close to the nucleus and this inner structure exhibits the main distinguishable features that helped to classify them *taxonomically* in terms of new (K,T) quantum labels [41–43]. Similarly we use this bound-like part of the resonances to calculate and analyze theoretic-information quantities. It is worth noting that for atoms with low nuclear charge, strong electron correlation is the basic characteristics within the Rydberg series of DES (the Coulomb repulsion term $1/r_{12}$ is responsible for their autoionization decay process into the continuum), in contrast to singly excited states. DES in helium have been the object of numerous resonance classification schemes (see [44] for a critical review) and they are good candidates to assess information, entanglement, and complexity measures as the benchmark of fermionic bipartite atomic systems.

DES in atoms and molecules represent a paradigmatic case for the understanding of the role of electron correlation. The ground state and single excitations are widely represented using the independent-particle model (IPM), in which the LS-coupled two-electron state with parity π is represented by the labels $|(n_1\ell_1,n_2\ell_2);^{2S+1}L^\pi\rangle$, since in their configuration mixing there is usually a leading IPM configuration. However, DES show a strong configuration interaction with the admixture of many IPM configurations and, as a general rule, without leading ones. This property led to new ways of classifying DES [40]. By combining the angular momenta ℓ_1 and ℓ_2 for a fixed pair (n_1,n_2) Herrick and Sinanoğlu [41,45] introduced group theory based new angular quantum numbers (K,T) in such a way that the new basis vectors, $|_{n_1}(K,T)_{n_2};^{2S+1}L^\pi\rangle$, called doubly excited symmetry basis (DESB) states were *almost* able to diagonalize the Hamiltonian, in a clear attempt of recovering again leading configurations, now in terms of the DESB. Nevertheless, since DESB are constructed for a given couple (n_1,n_2) with $n_2 \geqslant n_1$[n_1 indicating the inner electron and n_2 the outer electron], these basis states only describe restricted intrashell ($n_1 = n_2$) or intershell (n_1 fixed and $n_2 > n_1$) electron correlations. A CI method improves the description of each DES by combining many additional intra- and intershell excited configurations [with higher (n_1,n_2) pairs]. These new quantum numbers (K,T) remained in the subsequent classification by Lin [42,46] (by analyzing isomorphic correlations with hyperspherical coordinates), now representing angular labels for asymptotic dipole states, plus a new quantum number A, additionally introduced to account for radial correlation, to end up with a descriptor label $|_{n_1}(K,T)^A_{n_2};^{2S+1}L^\pi\rangle$.

To avoid lengthening the paper and unnecessary discussions on benchmark values, we only give Shannon entropies in tabulated form and the Fisher information and von Neumann entropies are given in graphical form. Although linear entropies have also been computed systematically, their results run parallel to the von Neumann entropies, which does not bring new insights into our analysis. The paper is organized as follows: In Sec. II we describe our theoretical approach, with (i) the procedure to compute the reduced spatial density $\rho(\mathbf{r})$ as well as the one-particle reduced density matrix $\hat{\rho}$ from CI wave functions, from which all theoretic-information entities can be calculated, and (ii) a short description of our implementation of the Feshbach approach to obtain the resonance wave functions as well as a description of DESB states. Section III is dedicated to the separate presentation and discussion of results for Shannon entropies, Fisher information, and entanglement measures. We end up with some conclusions and perspectives in Sec. IV. Atomic units (a.u.) are used throughout unless otherwise stated.

II. THEORY

A. Methodology

The electronic structure of the He atom is solved at the level of the configuration interaction (CI) method, to obtain accurate wave functions of the form [in our notation $\mathbf{x}_i = (\mathbf{r}_i,\sigma_i)$, $\mathbf{r}_i = (r_i,\Omega_i)$, and $\Omega_i = (\theta_i,\phi_i)$]

$$
\begin{aligned}
&{}^{2S+1}\Psi^\pi_{L,M}(\mathbf{x}_1,\mathbf{x}_2)\\
&\quad= \sum_{n_1\ell_1,n_2\ell_2} C_{n_1\ell_1,n_2\ell_2}\mathcal{A}\{\phi_{n_1\ell_1}(r_1)\phi_{n_2\ell_2}(r_2)\\
&\qquad\times\mathcal{Y}_{(\ell_1,\ell_2)L,M}(\Omega_1,\Omega_2)^{2S+1}\chi(\sigma_1,\sigma_2)\},
\end{aligned}
\tag{1}
$$

where $\mathcal{A}$ is the antisymmetrizer operator, $\mathcal{Y}_{(\ell_1,\ell_2)L,M}(\Omega_1,\Omega_2)$ corresponds to the bipolar spherical harmonic of angular coupling, π corresponds to the state parity, and ${}^{2S+1}\chi(\sigma_1,\sigma_2)$ is the two-electron spin eigenfunction for total spin S. The

variational expansion coefficients $C_{n_1\ell_1,n_2\ell_2}$ are obtained by numerically solving the eigenvalue problem associated with the two-electron Hamiltonian

$$\mathcal{H} = h_1 + h_2 + \frac{1}{r_{12}}. \tag{2}$$

In the expansion (1) the one-particle wave functions $\phi_{n\ell}(\mathbf{r}) = \mathcal{P}_{n\ell}(r)/r \cdot \mathcal{Y}_{\ell m}(\Omega)$ are chosen as eigenfunctions of the hydrogen-like Hamiltonian $h_i = -\nabla_i^2/2 - Z/r_i$ from Eq. (2). As in previous works [47], the reduced radial wave function $\mathcal{P}_{n\ell}(r)$ is expanded in terms of M B-splines basis functions $B_i^k(r)$. Once the CI wave function is obtained for a given state, the two-electron distribution function $\rho(\mathbf{u}_1,\mathbf{u}_2)$ corresponds to the expectation value of the operator $\hat{G}(\mathbf{u}_1,\mathbf{u}_2)$, i.e., $\rho(\mathbf{u}_1,\mathbf{u}_2) = \langle {}^{2S+1}\Psi^{\pi}_{LM}|\hat{G}(\mathbf{u}_1,\mathbf{u}_2)|{}^{2S+1}\Psi^{\pi}_{LM}\rangle$, which has the following form in the position representation for an atom or ion with N electrons [48]:

$$\hat{G}(\mathbf{u}_1,\mathbf{u}_2) = \sum_{i<j}^{N} \frac{1}{2}[\delta(\mathbf{r}_i - \mathbf{u}_1)\delta(\mathbf{r}_j - \mathbf{u}_2) + \delta(\mathbf{r}_i - \mathbf{u}_2)\delta(\mathbf{r}_j - \mathbf{u}_1)]. \tag{3}$$

After integrating over the irrelevant three Euler angles that determine the orientation of the triangle electron-nucleus-electron in space, the reduced operator reads

$$\hat{G}(u_1,u_2,\theta) = \sum_{i<j}^{N} \frac{1}{2}[\delta(r_i - u_1)\delta(r_j - u_2) + \delta(r_i - u_2)\delta(r_j - u_1)]\delta(cos\theta_{ij} - cos\theta), \tag{4}$$

and the corresponding two-electron density becomes $\rho(u_1,u_2,\theta) = \langle {}^{2S+1}\Psi^{\pi}_{LM}|\hat{G}(u_1,u_2,\theta)|{}^{2S+1}\Psi^{\pi}_{LM}\rangle$. For instance, using standard tensor algebra, the matrix element of the reduced density operator between two non-antisymmetrized two-electron configurations $\langle\hat{G}(r_1,r_2,\theta)\rangle_{ab,cd} = \langle(n_a\ell_a)_1(n_b\ell_b)_2LS|\hat{G}(u_1,u_2,\theta)|(n_c\ell_c)_1(n_d\ell_d)_2LS\rangle$ has the form

$$\begin{aligned}(\hat{G}(r_1,r_2,\theta))_{ab,cd} &= R(ab,cd)\sum_k \frac{1}{4}(-1)^{L-k}(2k+1) \\ &\times [(2l_a+1)(2l_b+1)(2l_c+1)(2l_d+1)]^{\frac{1}{2}} \\ &\times \begin{pmatrix} l_a & l_c & k \\ 0 & 0 & 0 \end{pmatrix}\begin{pmatrix} l_b & l_d & k \\ 0 & 0 & 0 \end{pmatrix}\begin{Bmatrix} l_a & k & l_c \\ l_d & L & l_b \end{Bmatrix} P_k(cos\theta),\end{aligned} \tag{5}$$

where $P_k(\cos\theta)$ is a Legendre polynomial and, at variance with the $1/r_{12}$ operator, the radial integral $R(ab,cd)$ does not depend on the k index and its value is straightforwardly obtained after radial integration

$$R(ab,cd) = \mathcal{P}_{n_a\ell_a}(u_1)\mathcal{P}_{n_b\ell_b}(u_2)\mathcal{P}_{n_c\ell_c}(u_1)\mathcal{P}_{n_d\ell_d}(u_2) + \mathcal{P}_{n_a\ell_a}(u_2)\mathcal{P}_{n_b\ell_b}(u_1)\mathcal{P}_{n_c\ell_c}(u_2)\mathcal{P}_{n_d\ell_d}(u_1). \tag{6}$$

Our final expression for the reduced spatial density is completely equivalent to that quoted in Ref. [43], which was obtained by other means. Finally, the radial two-electron density distribution is calculated by trivial angular integration

$$\rho(u_1,u_2) = \int_{-1}^{+1} d(\cos\theta)\rho(u_1,u_2,\theta), \tag{7}$$

and the one-electron radial density by additionally integrating over one radial coordinate, for instance u_2,

$$\rho(u) = \int_0^{\infty} u_2^2 du_2 \int_{-1}^{+1} d(\cos\theta)\rho(u_1 = u,u_2,\theta). \tag{8}$$

Henceforth, for the sake of clarity, we replace the notation $\mathbf{u} \to \mathbf{r}$ for the electron coordinates in the density expressions.

The Shannon entropy for discrete distributions is defined in information theory as $S = -\sum_i p_i \ln p_i$ with $\sum_i p_i = 1$. For continuous distributions the definition is $S = -\int d\mathbf{r} f(\mathbf{r}) \ln f(\mathbf{r})$, with $\int d\mathbf{r} f(\mathbf{r}) = 1$. In the usual definition, the integral of the one-electron density yields the number of electrons in the atom, but according to information theory we instead choose to normalize the radial density to unity, i.e., $\int d\mathbf{r}\rho(r) = 1$. Similarly, the two-electron radial density is also renormalized to unity. With these two distributions we can compute the Shannon entropy for the two-electron radial distribution $S_2 = -\int d\mathbf{r}_1 \int d\mathbf{r}_2 \rho(r_1,r_2)\ln\rho(r_1,r_2)$, or for the one-electron distribution $S_1 = -\int d\mathbf{r}\rho(r)\ln\rho(r)$.[1] We found (see also results on the Hooke's atom [6]) that both entropies S_1 and S_2 show a similar qualitative trend for ${}^{1,3}L^e$ ($L = 0,1,2$) bound states in He, so that (for easier calculation) we only report S_1-like Shannon entropies for both bound states and DES. In this case it reduces to evaluating the expression

$$S[\rho] = -4\pi \int_0^{\infty} r^2\rho(r)\ln\rho(r), \tag{9}$$

by using numerical quadrature integration. The Fisher information is defined by the two equivalent expressions

$$I[\rho] = \int d\mathbf{r}|\nabla \ln\rho(\mathbf{r})|^2\rho(\mathbf{r}) = \int d\mathbf{r}\frac{|\nabla\rho(\mathbf{r})|^2}{\rho(\mathbf{r})}. \tag{10}$$

It is worth noting that the Fisher information is related to the von Weisäcker inhomogeneity kinetic-energy correction term $\hbar^2|\nabla\rho|^2/8m\rho$ (not in a.u.) in density functional theory [49] and also to Bohm's quantum potential [50,51].

Entanglement in two-electron systems is related to the Schmidt-Slater decomposition of a pure state $|\Psi\rangle$ [52], in terms of an orthonormal basis of one-particle states $\{|\phi_i\rangle\}$ in the form

$$|\Psi\rangle = \sum_i \sqrt{\frac{\lambda_i}{2}}[|\phi_{2i}(1)\rangle|\phi_{2i+1}(2)\rangle - |\phi_{2i+1}(1)\rangle|\phi_{2i}(2)\rangle], \tag{11}$$

where the set of Schmidt-Slater coefficients $\{\lambda_i\}$ satisfies $0 \leqslant \lambda_i \leqslant 1$ and $\sum_i \lambda_i = 1$. The number of nonzero Schmidt-Slater coefficients defines the Slater rank of the state. If the Slater rank equals unity (only one Slater determinant) the

[1] One-electron radial density can be straightforwardly obtained using the operator $\hat{G} = \sum_{i=1}^{N}\delta(\mathbf{r} - \mathbf{r}_i)$, then used in the Shannon entropy S_1. In this work we began by studying both Shannon entropies S_1 and S_2, using the two-electron radial density.

state is not entangled. It is known that these Schmidt-Slater coefficients are related to the eigenvalues of the one-particle reduced density matrix [53], and from this, measures of the amount of entanglement $\mathcal{E}$ in the pure state $|\Phi\rangle$ have been proposed [11,19,21,29] in the general form for N fermions as

$$\mathcal{E}_L = N\left[S_L(\hat{\rho}) - \left(\frac{N-1}{N}\right)\right], \tag{12}$$

in terms of the standard linear entropy $S_L(\hat{\rho}) = 1 - \mathrm{Tr}[\hat{\rho}^2]$, and where the term $(N-1)/N$ eliminates the contribution to the linear entropy only due to antisymmetrization, or

$$\mathcal{E}_{VN} = S_{VN}[\hat{\rho}] - \log_2 N, \tag{13}$$

using the standard von Neumann entropy $S_{VN}[\hat{\rho}] = -\mathrm{Tr}[\hat{\rho}\log_2\hat{\rho}]$ and the term $\log_2 N$ similarly cancels the nonessential entanglement content due to the antisymmetrization. For two electrons ($N = 2$) these expressions reduce to $\mathcal{E}_L = 1 - 2\mathrm{Tr}[\hat{\rho}^2]$ and $\mathcal{E}_{VN} = S_{VN}[\hat{\rho}] - 1$. Now, due to the separability of the spatial and spin parts in the two-electron total wave function (1), the reduced density matrix can be expressed as a product of reduced density matrices ($\hat{\rho} = \hat{\rho}^{\mathrm{spatial}} \otimes \hat{\rho}^{\mathrm{spin}}$), which transforms the entanglement measures (12) and (13) into

$$\mathcal{E}_L = 1 - 2\mathrm{Tr}[(\hat{\rho}^{\mathrm{spatial}})^2]\mathrm{Tr}[(\hat{\rho}^{\mathrm{spin}})^2] \tag{14}$$

and

$$\mathcal{E}_{VN} = S_{VN}[\hat{\rho}^{\mathrm{spin}}] + S_{VN}[\hat{\rho}^{\mathrm{spatial}}] - 1. \tag{15}$$

In this work we only select those spin singlet and triplet states of the entangled Bell-wise form ${}^{1,3}\chi(1,2) = \frac{1}{\sqrt{2}}[\alpha(1)\beta(2) \mp \beta(1)\alpha(2)]$, which satisfy $\mathrm{Tr}[(\hat{\rho}^{\mathrm{spin}})^2] = 1/2$ and $S_{VN}[\hat{\rho}^{\mathrm{spin}}] = 1$, and from which one readily finds that $\mathcal{E}_L \equiv S_L[\hat{\rho}^{\mathrm{spatial}}]$ and $\mathcal{E}_{VN} \equiv S_{VN}[\hat{\rho}^{\mathrm{spatial}}]$; i.e., entanglement measures $\mathcal{E}_L$ and $\mathcal{E}_{VN}$ (including spin and cancellations due to simple antisymmetrization) coincide with the standard spatial linear entropy $S_L(\hat{\rho}^{\mathrm{spatial}})$ and the standard spatial von Neumann entropy $S_{VN}(\hat{\rho}^{\mathrm{spatial}})$, respectively, with this choice of spin wave function. Accordingly, we use in the following the standard von Neumann and linear entropies applied to the spatial part of the wave function as direct entanglement measures, which allows us to compare our numerical results with previous works on the He atom [19,29,30,32,33].

The standard spatial von Neumann entropy is defined through the expression (from now, $\hat{\rho}^{\mathrm{spatial}} \to \hat{\rho}$)

$$\begin{aligned} S_{VN}[\hat{\rho}] &= -\mathrm{Tr}[\hat{\rho}(\mathbf{r}_1,\mathbf{r}'_1)\log_2\hat{\rho}(\mathbf{r}_1,\mathbf{r}'_1)] \\ &= -\int d\mathbf{r}[\hat{\rho}(\mathbf{r},\mathbf{r})\log_2\hat{\rho}(\mathbf{r},\mathbf{r})], \end{aligned} \tag{16}$$

where $\hat{\rho}(\mathbf{r}_1,\mathbf{r}'_1)$ is the reduced density matrix of the subsystem electron 1 [not to be confused with the two-electron density distribution $\rho(\mathbf{r}_1,\mathbf{r}_2)$ introduced above], obtained after tracing the full two-electron density matrix in the coordinate representation [i.e., $\hat{\rho}(\mathbf{r}_1\mathbf{r}_2;\mathbf{r}'_1\mathbf{r}'_2) = \langle\mathbf{r}_1\mathbf{r}_2|\hat{\rho}|\mathbf{r}'_1\mathbf{r}'_2\rangle = \langle\mathbf{r}_1\mathbf{r}_2|\Psi_{CI}\rangle\langle\Psi_{CI}|\mathbf{r}'_1\mathbf{r}'_2\rangle$ obtained from the two-electron pure state $|\Psi_{CI}\rangle$ whose coordinate representation is in the form of Eq. (1)] over the coordinates of one subsystem (electron 2, for instance) to yield a reduced density matrix of a (usually) *mixed* state for electron 1 with the expression

$$\begin{aligned} \hat{\rho}(\mathbf{r}_1,\mathbf{r}'_1) &= \mathrm{Tr}_2\hat{\rho}(\mathbf{r}_1,\mathbf{r}_2;\mathbf{r}'_1,\mathbf{r}'_2) \\ &= \int d\mathbf{r}_2\Psi_{CI}(\mathbf{r}_1,\mathbf{r}_2)\Psi^*_{CI}(\mathbf{r}'_1,\mathbf{r}_2). \end{aligned} \tag{17}$$

The linear entropy is an approximation to the von Neumann entropy, obtained by expanding the logarithm in Eq. (16) in power series of the density matrix and keeping only the leading terms (along with the property $\mathrm{Tr}[\hat{\rho}] = 1$) to give

$$S_L[\hat{\rho}] = 1 - \mathrm{Tr}[\hat{\rho}^2(\mathbf{r}_1,\mathbf{r}'_1)] = 1 - \int d\mathbf{r}\hat{\rho}^2(\mathbf{r},\mathbf{r}), \tag{18}$$

where $\hat{\rho}^2(\mathbf{r}_1,\mathbf{r}'_1) = \int d\mathbf{r}_2\hat{\rho}(\mathbf{r}_1,\mathbf{r}_2)\hat{\rho}(\mathbf{r}_2,\mathbf{r}'_1)$ and $\mathrm{Tr}[\hat{\rho}^2]$ is called *purity*.

From the previous expressions for S_L and S_{VN} it might seem that the computation of these quantities require up to 12-dimensional integrals, which have been previously calculated using Monte Carlo numerical integration methods [19,29] using explicitly correlated Kinoshita-type basis functions, although they can be performed analytically when using explicitly correlated Hylleraas basis sets, as shown in [33]. Indeed we have experience in using Hylleraas-type basis sets in CI methods [54] but we have chosen an uncorrelated CI method that incorporates antisymmetrized products of orthogonal orbitals, which makes not only the application of the Feshbach projection method and the subsequent analysis in terms of DESB much more simple, but also the calculation of S_L and S_{VN} entropies. Using the CI expansion of Eq. (1) in terms of orthogonal orbitals, the representation of the two-electron density operator $\hat{\rho}(\mathbf{r}_1\mathbf{r}_2;\mathbf{r}'_1\mathbf{r}'_2)$ becomes $\hat{\rho}_{n_1\ell_1,n_2\ell_2;n'_1\ell'_1,n'_2\ell'_2} = C_{n_1\ell_1,n_2\ell_2}\cdot C^*_{n'_1\ell'_1,n'_2\ell'_2}$ and the one-electron reduced density matrix elements are straightforwardly obtained by taking the trace over the electron 2, in the form $\hat{\rho}_{n_1\ell_1;n'_1\ell'_1} = \sum_{n\ell} C_{n_1\ell_1,n\ell}C^*_{n'_1\ell'_1,n\ell}$ [55]. By carrying the matrix $\hat{\rho}_{n_1\ell_1;n'_1\ell'_1}$ to its diagonal form, the entropies can be calculated in the following two equivalent ways:

$$S_L = 1 - \sum_{n\ell,n'\ell'}\hat{\rho}_{n\ell;n'\ell'}\cdot\hat{\rho}_{n'\ell';n\ell} = 1 - \sum_{i=1}^{M}\lambda_i^2 \tag{19}$$

for the linear entropy, and with

$$S_{VN} = -\sum_{i=1}^{M}\lambda_i\log_2\lambda_i \tag{20}$$

for the von Neumann entropy, where $\{\lambda_i\}_{i=1}^M$ is the set of M eigenvalues of the one-electron reduced density matrix with the property $\sum_{i=1}^M\lambda_i = 1$. The value M corresponds to the size of the one-electron Hilbert space, i.e., the total number of orbitals $\phi_{n\ell}(r)$ used to build our CI wave functions in Eq. (1).

B. Resonances: Feshbach approach

The atomic resonances in He are DES with energies lying above the first ionization threshold and below the complete break-up double ionization threshold. They are true eigenstates

in the continuum spectra of the Hamiltonian in Eq. (2) showing a strong electron localization close to the nucleus. Since they are immersed in the electronic continuum, a direct diagonalization of the Hamiltonian cannot uncover the energy location of these resonances. Different methods have been proposed to characterize these resonance states, such as the stabilization method [56], the complex coordinate scaling [57], the Feshbach method [58], or scattering methods [59], among others, previously used by us in other contexts [54,60,61]. The Feshbach method is a projection operator formalism which separates the total resonance wave function Ψ (eigenfunction of $\mathcal{H}$) into two orthogonal half spaces: its bound-like part $\mathcal{Q}\Psi$ and its scattering-like part $\mathcal{P}\Psi$, such that $\Psi = \mathcal{Q}\Psi + \mathcal{P}\Psi$. For a fuller recent description of the Feshbach formalism and its application by us to two- and three-electron atoms see Refs. [47,61,62]. Here we only give a simple outline. The projected wave functions satisfy the asymptotic boundary conditions $\lim_{r_i\to\infty} \mathcal{P}\Psi = \Psi$ and $\lim_{r_i\to\infty} \mathcal{Q}\Psi = 0$, where the latter expression indicates the confined nature of the localized part of the resonance. Since any useful *taxonomy* to classify different resonances depends mainly on the localized bound-like part and not on the scattering-like part, which is basically common to all of them, it suffices to analyze the projected wave function in the $\mathcal{Q}$ half space. In our approach to the Feshbach method the $\mathcal{Q}\Psi$ wave function is an eigenstate of the projected Hamiltonian $\mathcal{QHQ}$, i.e., $(\mathcal{QHQ} - \mathcal{E})\mathcal{Q}\Psi = 0$, where for the two-electron case $\mathcal{Q} = \mathcal{Q}_1\mathcal{Q}_2$ and $\mathcal{P} = 1 - \mathcal{Q}$, with $\mathcal{Q}_i = 1 - \mathcal{P}_i$ $(i = 1,2)$. Then the full projector $\mathcal{P} = \mathcal{P}_1 + \mathcal{P}_2 - \mathcal{P}_1\mathcal{P}_2$ accounts for the antisymmetry. The explicit form of the one-particle $\mathcal{P}_i$ projector depends on which Rydberg series of resonances we are interested in. In this work we restrict our study to DES located above the first ionization threshold $He^+(1s)$ and below the second ionization threshold $He^+(2s,2p)$, then embedded in a continuum of the form $He(1s\varepsilon\ell)$, with ε being the excess energy of the scattering electron above the first ionization threshold. In this particular case the one-particle projector is simply $\mathcal{P}_i = |\phi_{1s}(i)\rangle\langle\phi_{1s}(i)|$ and with it the corresponding $\mathcal{Q}$ projector has the effect of removing all those configurations in the CI wave function (1) containing the $1s$ orbital, then avoiding the variational collapse to the ground state $He(\sim 1s^2)$, to singly excited states $He(\sim 1sn\ell)$ and the single ionization continuum $He(\sim 1s\varepsilon\ell)$. As a result, the lowest variational energies of the $\mathcal{QHQ}$ eigenvalue problem correspond to a square-integrable $(\mathcal{L}^2)$ discrete set of DES or resonances, devoid of any scattering-like participation.

C. The DESB states

The doubly excited symmetry basis (DESB) states [41,45] are characterized by the two quantum labels K and T, and they are obtained by a linear superposition of hydrogen-like IPM configurations as follows:

$$|_{n_1}(K,T)_{n_2};^{2S+1}L^\pi\rangle = \sum_{\ell_1\ell_2} |n_1\ell_1 n_2\ell_2;^{2S+1}L^\pi\rangle \mathcal{D}^{KTL\pi}_{n_1\ell_1 n_2\ell_2}, \tag{21}$$

where $|n_1\ell_1 n_2\ell_2;^{2S+1}L^\pi\rangle$ corresponds to an antisymmetrized configuration as used in Eq. (1), and $\mathcal{D}$ is proportional to a Wigner 9-j factor, as follows:

$$\begin{aligned} D^{KTL\pi}_{n_1\ell_1 n_2\ell_2} &= M(T,\pi)\times(-1)^{\ell_2}[(n_2+K+T)(n_2+K-T) \\ &\quad\times(2\ell_1+1)(2\ell_2+1)]^{1/2} \\ &\quad\times\begin{Bmatrix} (n_1-1)/2 & (n_2-1)/2 & (n_2-1+K+T)/2 \\ (n_1-1)/2 & (n_2-1)/2 & (n_2-1+K-T)/2 \\ \ell_1 & \ell_2 & L \end{Bmatrix}, \end{aligned} \tag{22}$$

where $M(T,\pi)$ is a normalization factor [$M = 1$ if $T = 0$, $M = \sqrt{2}$ if $T > 0$, and $M = 0$ unless $(-1)^{\ell_1+\ell_2} = \pi$]. DESB states are eigenfunctions of the operator $\hat{B}^2 = n_2(\hat{A}_1 - \hat{A}_2)^2$, where $\hat{A}_i$ is the Runge-Lenz operator for electron i. The amazing result is that the operator $\hat{B}^2$ almost commutes with the two-electron interaction $1/r_{12}$ in Eq. (2) and thus DESB states are *almost* the Hamiltonian eigenstates. Ultimately, this means that if resonant DES are more properly described with DESB states, the resonance Rydberg series given by $|_{n_1}(K,T)_{n_2};^{2S+1}L^\pi\rangle$ (for a fixed n_1, then increasing $n_2 > n_1$ up to ∞) contain indeed several Rydberg series in terms of IPM hydrogen-like configurations. For example, the two $_2(K,T)_{n_2}$ series in $^{1,3}S^e$ states are obtained from combinations of the two hydrogen-like Rydberg series $2sn_2s$ and $2pn_2p$ as follows:

$$|_2(\pm 1,0)_{n_2};\,^{1,3}S^e\rangle = \left[\frac{n_2 \pm 1}{2n_2}\right]^{1/2} |2sn_2s\rangle \pm \left[\frac{n_2 \mp 1}{2n_2}\right]^{1/2} |2pn_2p\rangle. \tag{23}$$

Similarly, in the $^{1,3}P^o$ symmetry the $_2(\pm 1,0)_{n_2}$ DESB states are combinations of three hydrogen-like Rydberg series with fixed $n_1 = 2$ and with $n_2 \geqslant 2$, in the form

$$\begin{aligned} |_2(\pm 1,0)_{n_2};\,^{1,3}P^o\rangle &= \left[\frac{(n_2 \mp 1)(n_2 \pm 2)}{2n_2^2}\right]^{1/2} |2sn_2p\rangle \\ &\quad \mp \left[\frac{(n_2 \pm 1)(n_2 \pm 2)}{6n_2^2}\right]^{1/2} |2pn_2s\rangle \\ &\quad \pm \left[\frac{(n_2 \mp 1)(n_2 \mp 2)}{3n_2^2}\right]^{1/2} |2pn_2d\rangle. \end{aligned} \tag{24}$$

Herrick and Sinanoğlu found that if the complete set of DESB states is used as a basis to expand the total wave function, each DES coming from the Hamiltonian diagonalization is dominated by DESB states with the same values of the labels K and T. Therefore, on these grounds, it is expected that theoretic-information properties of highly lying $^{1,3}P^o$ DES will not show clear limiting values corresponding to single residual ionic states [$He^+(2s)$ or $He^+(2p)$], but to an intricate mixture.

When neglecting the $1/r_{12}$ interaction, the energy of a two-electron hydrogen-like atomic system is $E_{n_1,n_2} = -\frac{Z^2}{2}(\frac{1}{n_1^2} + \frac{1}{n_2^2})$ and then simple IPM configurations $(n_1\ell_1, n_2\ell_2)$ (with $n_1 = 2$ and $n_2 \geqslant 2$) built from hydrogen-like orbitals are exact eigenstates of the Feshbach $\mathcal{QHQ}$ projected Hamiltonian. In this case, for example, intrashell IPM configurations $\{2s2s, 2p2p\}$ entering in Eq. (23) with $n_2 = 2$ or intershell

IPM configurations $\{2s3p,2p3s,2p3d\}$ in Eq. (24) with $n_2 = 3$ form energy degenerated manifolds. With $1/r_{12}$ included, the energy degeneration of both intrashell ($n_1 = n_2$) and intershell ($n_1 < n_2$) hydrogenic IPM configurations entering in the right-hand side of Eq. (21) is exact only at $Z = \infty$, which justifies their linear combination within each degenerated manifold to build DESB states; this degeneracy is lifted for any finite Z. Approximate DESB states may be obtained numerically at any Z value as the eigenstates resulting from diagonalizing the $1/r_{12}$ interaction in the set of intra- or intershell IPM configurations compatible with the total $^{2S+1}L^{\pi}$ symmetry. The expansion coefficients of the latter eigenstates are closer to those of the DESB as $Z \to \infty$, and also in this limit they come closer to those from *ab initio* full CI calculations, because intershell interactions tend to vanish for $Z \to \infty$ due to the increasing energy separation among atomic shells. From this perspective, DES in He may be thought of as a particularly realistic example of the effect of energy degeneracy in the non-interacting limit, lifted by the electron repulsion term $1/r_{12}$, an interaction that already produces a mixing of the degenerate states if we build the zeroth-order wave function according to degenerate perturbation theory [21], then inducing a nonzero entanglement even in the noninteracting limit. Consequently, DES in He, in contrast to singly excited states, may always show a given degree of entanglement from low to very high excitation as an intrinsic property of these resonant states, independent of the entanglement measure used.

III. RESULTS

We first compute the energies and wave functions of bound states of helium using our CI method based on a B-splines basis expansion. To keep the number of configurations closer to the full CI with a reasonably small number of orbitals we use 40 B-splines per angular momentum ℓ distributed in an exponential grid (well suited to represent localized states, at variance with our previous work where a linearly distributed grid was used [47], intended to also represent the two-electron continuum states) within a box of size $L = 200$ a.u. $^1S^e$ states are computed using 820 $nsn's$ configurations ($n,n' = 1$–40), 820 $npn'p$ configurations ($n,n' = 2$–41), 820 $ndn'd$ ($n,n' = 3$–42), 820 $nfn'f$ ($n,n' = 4$–43), 820 $ngn'g$ ($n,n' = 5$–44), and 820 $nhn'h$ ($n,n' = 6$–45), which represents a full CI with 4920 configurations. The $^1P^o$ states are calculated with 6400 configurations (including sp, pd, df, and fg). Similarly, the $^1D^e$ symmetry is computed with 7529 configurations (sd, pp, pf, dd, dg, ff, and gg). The triplet states are computed using 4680 configurations for $^3S^e$, 6400 for $^3P^o$, and 5306 for $^3D^e$. Table I summarizes the energies obtained for the lowest series of bound states in these six spectroscopic symmetries.

We have also performed CI calculations for the DES by diagonalizing the projected Hamiltonian $\mathcal{QHQ}$, with the same configuration basis set used for bound states, but now, in practice, projecting out the $1s$ orbital. We are able to obtain, lying below the second ionization threshold $He^+(n_1 = 2)$, 23 DES of symmetry $^1S^e$, 32 states for $^1P^o$, and 30 states for $^1D^e$, using 4880, 6360, and 7489 configurations, respectively. On the other hand, we get 21 DES of symmetry $^3S^e$, 32 DES for $^3P^o$, and 29 DES for $^3D^e$, by using 4641, 6360, and 5266 configurations, respectively. Nevertheless, only the lowest ones (6–7 in each symmetry) are converged in energy within 5–6 figures. The comparison of our calculated DES energies, reported in Table II, with the very precise values calculated by Chen [63], using the saddle-point complex rotation method, is very reasonable. The deviations from the values given in Ref. [63] are mostly due to the fact that the energy correction due to the surrounding continuum states (the energy shift) is not included in our results.

TABLE I. Energies (in a.u.) and Shannon entropies S of the lowest bound states $1sn\ell\,^{1,3}L^{\pi}$ (with $\ell = L$) of helium, below the first ionization threshold $He^+(n = 1)$ ($E = -2.0$ a.u.) for the spectroscopic symmetries $^{1,3}S^e$, $^{1,3}P^o$, and $^{1,3}D^e$ obtained in this work.

	$^1S^e$		$^1P^o$		$^1D^e$	
state	E (a.u.)	S	E (a.u.)	S	E (a.u.)	S
$1s1\ell$	−2.903605	2.705				
$1s2\ell$	−2.145967	5.492	−2.123823	5.515		
$1s3\ell$	−2.061270	6.769	−2.055140	6.817	−2.055620	6.635
$1s4\ell$	−2.033586	7.645	−2.031067	7.695	−2.031280	7.596
$1s5\ell$	−2.021176	8.310	−2.019905	8.359	−2.020016	8.295
$1s6\ell$	−2.014563	8.856	−2.013833	8.903	−2.013898	8.853
$1s7\ell$	−2.010626	9.330	−2.010169	9.371	−2.010210	9.329
$1s8\ell$	−2.008093	9.663	−2.007788	9.688	−2.007816	9.656
$1s9\ell$	−2.006360	9.681	−2.006141	9.675	−2.006164	9.667
$1s10\ell$	−2.004961	9.626	−2.004754	9.689	−2.004801	9.549
	$^3S^e$		$^3P^o$		$^3D^e$	
state	E (a.u.)	S	E (a.u.)	S	E (a.u.)	S
$1s2\ell$	−2.175229	5.236	−2.133162	5.356		
$1s3\ell$	−2.068689	6.605	−2.058080	6.722	−2.055635	6.634
$1s4\ell$	−2.036512	7.523	−2.032324	7.628	−2.031288	7.596
$1s5\ell$	−2.022619	8.217	−2.020551	8.307	−2.020021	8.294
$1s6\ell$	−2.015377	8.775	−2.014208	8.859	−2.013901	8.852
$1s7\ell$	−2.011130	9.254	−2.010405	9.335	−2.010212	9.329
$1s8\ell$	−2.008427	9.601	−2.007947	9.664	−2.007818	9.655
$1s9\ell$	−2.006596	9.675	−2.006256	9.672	−2.006165	9.667
$1s10\ell$	−2.005183	9.502	−2.004870	9.613	−2.004801	9.548

To assess our radial two-electron density distributions $\rho(r_1,r_2)$, quoted in Eq. (7), we plot in Fig. 1 these radial distributions for the lowest three members of each ${}_{n_1}(K,T)_{n_2}$ series in the symmetry $^1P^o$, ${}_2(0,1)^+_{n_2}$, with $n_2 = 2,3,4$; ${}_2(1,0)^-_{n_2}$, with $n_2 = 3,4,5$; and ${}_2(-1,0)_{n_2}$ with $n_2 = 3,4,5$. The energy ordering of DES is given by the prefix N in the notation $N\,^1P^o$, ranging from $N = 1$ to 10 (the corresponding energies are included in Table II). Clearly the second series with $A = -1$ displays a node for $r_1 = r_2$, absent in the first series with $A = +1$ and not evident with $A = 0$. Also the number of radial nodes along any of the two radial coordinates increases with the excitation within each series. In fact, the lowest member in each series has no radial nodes in the r_1 or r_2 direction below or above the bisection line given by $r_1 = r_2$, a property typical of ground states. Density plot analyses have been carried out in the past, like in Ref. [43] for $\rho(r_1,r_2,\theta)$, by making cuts at a given radial distance ($r_2 = \alpha$), but to our knowledge only a reference with radial density plots $\rho(r_1,r_2)$ for DES in He is available [64]. In the latter work the authors calculated a multipolar series expansion of the full density

TABLE II. Energy positions (in a.u.) (without energy shift correction) and Shannon entropies S of the lowest resonant doubly excited states of helium located below the second ionization threshold $He^+(n_1 = 2)$ for the total symmetries $^{1,3}S^e$, $^{1,3}P^o$, and $^{1,3}D^e$. Resonances are labeled according to the classification proposed by Lin [46] using ${}_{n_1}(K,T)^A_{n_2}$; $^{2S+1}L^\pi$. The superscript notation $+,-$ in S and D symmetries must be understood as $A = +1$ for the singlets and $A = -1$ for triplet states.

	$^1S^e$		$^3S^e$	
	Energy (a.u.)	S	Energy (a.u.)	S
${}_2(1,0)^{+,-}_2$	−0.778775	6.380		
${}_2(1,0)^{+,-}_3$	−0.590099	8.136	−0.602601	7.974
${}_2(1,0)^{+,-}_4$	−0.544939	9.133	−0.548848	9.043
${}_2(1,0)^{+,-}_5$	−0.526707	9.874	−0.528417	9.821
${}_2(1,0)^{+,-}_6$	−0.517650	10.46	−0.518548	10.44
${}_2(-1,0)^{+,-}_2$	−0.622559	6.874		
${}_2(-1,0)^{+,-}_3$	−0.548216	8.786	−0.559765	8.418
${}_2(-1,0)^{+,-}_4$	−0.527781	9.728	−0.532512	9.437
${}_2(-1,0)^{+,-}_5$	−0.518140	10.41	−0.520552	10.16
${}_2(-1,0)^{+,-}_6$	−0.512785	10.95	−0.514182	10.73
	$^1P^o$		$^3P^o$	
	Energy (a.u.)	S	Energy (a.u.)	S
	${}_2(0,1)^+_{n_2}$		${}_2(1,0)^+_{n_2}$	
$n_2 = 2$	−0.692754	6.546	−0.761484	6.349
$n_2 = 3$	−0.564010	8.400	−0.584929	8.146
$n_2 = 4$	−0.534332	9.372	−0.542932	9.166
$n_2 = 5$	−0.521488	10.08	−0.525756	9.924
$n_2 = 6$	−0.514724	10.64	−0.517131	10.52
	${}_2(1,0)^-_{n_2}$		${}_2(0,1)^+_{n_2}$	
$n_2 = 3$	−0.597095	7.970	−0.579030	8.077
$n_2 = 4$	−0.546486	8.910	−0.539558	9.152
$n_2 = 5$	−0.527293	9.729	−0.523946	9.912
$n_2 = 6$	−0.517935	10.35	−0.516079	10.50
$n_2 = 7$	−0.512678	10.86	−0.511547	10.99
	${}_2(-1,0)^0_{n_2}$		${}_2(-1,0)^+_{n_2}$	
$n_2 = 3$	−0.547091	8.917	−0.548854	8.5385089
$n_2 = 4$	−0.527614	9.771	−0.528643	9.4961463
$n_2 = 5$	−0.518116	10.42	−0.518712	10.199407
$n_2 = 6$	−0.512790	10.95	−0.513157	10.761879
	$^1D^e$		$^3D^e$	
	Energy (a.u.)	S	Energy (a.u.)	S
${}_2(1,0)^{+,-}_2$	−0.702699	6.380		
${}_2(1,0)^{+,-}_3$	−0.569369	8.272	−0.583795	7.999
${}_2(1,0)^{+,-}_4$	−0.536785	9.286	−0.541681	9.098
${}_2(1,0)^{+,-}_5$	−0.522771	10.03	−0.525019	9.879
${}_2(1,0)^{+,-}_6$	−0.515470	10.61	−0.516688	10.49
${}_2(0,1)^0_3$	−0.556414	8.447	−0.560662	8.248
${}_2(0,1)^0_4$	−0.531505	9.447	−0.533448	9.320
${}_2(0,1)^0_5$	−0.520114	10.17	−0.521123	10.08
${}_2(0,1)^0_6$	−0.513950	10.74	−0.514536	10.66
${}_2(-1,0)^0_4$	−0.529173	9.309	−0.529288	9.303
${}_2(-1,0)^0_5$	−0.518937	10.08	−0.518998	10.07
${}_2(-1,0)^0_6$	−0.513273	10.66	−0.513309	10.65

$\rho(\mathbf{r}_1,\mathbf{r}_2) = \sum_{\ell\ell' m} \rho_{\ell m \ell' m}(r_1,r_2)\mathcal{Y}_{\ell m}(\Omega_1)\mathcal{Y}^*_{\ell' m}(\Omega_2)$, in such a form that the lowest radial coefficient $\rho_{0000}(r_1,r_2)$ describes the angle-averaged relative radial probability, which is proportional to our calculated density $\rho(r_1,r_2)$. The comparison of the density contour plots in Fig. 3 of Ref. [64] for the lowest $^1P^o$ resonances in He with ours in Fig. 1 is excellent.[2] One-particle radial densities $\rho(r)$ are then obtained by integrating these distributions $\rho(r_1,r_2)$ over one of the electron coordinates. A very good agreement of our one-particle radial densities for bound states in He with those available in Ref. [65] validates our computational approach for the densities.

A. Shannon entropy

The Shannon entropy is known exactly for a few quantum systems, with available analytical expressions for the one-particle density. For instance, the Shannon entropy for the ground state of the hydrogen atom is simply $S = 3 + \ln\pi = 4.14473$ [66]. We have reproduced this value for the ground state of hydrogen and also obtained numerical values for other Rydberg states, using our computed hydrogen-like orbitals entering in the CI method. The Shannon entropy augments with the increasing delocalization in the electron distribution. Accordingly the Shannon entropy exhibits a minimum for the compactly localized density of ground states and maximal for uniform distributions like those corresponding to the structureless *plane-wave*-like continuum. Since the upper limit in the radial integral of the Shannon entropy is infinity and the spatial radial extension of the states in the Rydberg series increases with excitation energy, the first ionization threshold of any atomic system might represent an asymptote for the Shannon entropy of bound states. Consequently, the Shannon entropy values for the singly excited states (singlets and triplets) of helium atom quoted in Table I can be easily understood. The Shannon entropy increases monotonically with single excitation, from the lowest value, corresponding to the lowest eigenstate of each symmetry (with the most compact density) to infinity when the energy approaches the first ionization threshold $He^+(1s)$. Our computation has limitations due to the number of configurations and the length of the box used to define our basis set of B splines. The number of bound Rydberg states obtained in the diagonalization strongly depends on these two parameters. Our box length ($L = 200$ a.u.) cannot accommodate the full extension of the radial distribution of highly excited Rydberg states $1s n\ell$ for $\ell > 9$ and thus we only report a limited number of bound singly excited states. Because of this limitation, our Shannon entropies in Table I seem to converge to a fixed value around ∼9.7. Actually, better calculations would show that Shannon entropy must increase indefinitely with further excitation to eventually diverge at the ionization threshold $E(He^+[n = 1]) = -2.0$ a.u.

From the energies and Shannon entropies for He bound states in Table I we are tempted to use this entity to predict the energy ordering. In fact, this prediction is very

[2]Note that in Ref. [64] the energy ordering for the Feshbach resonances $7\,^1P^o(1,0)$ and $8\,^1P^o(-1,0)$ must be exchanged. Other more recent and our present calculations are much more accurate than those performed at that time.

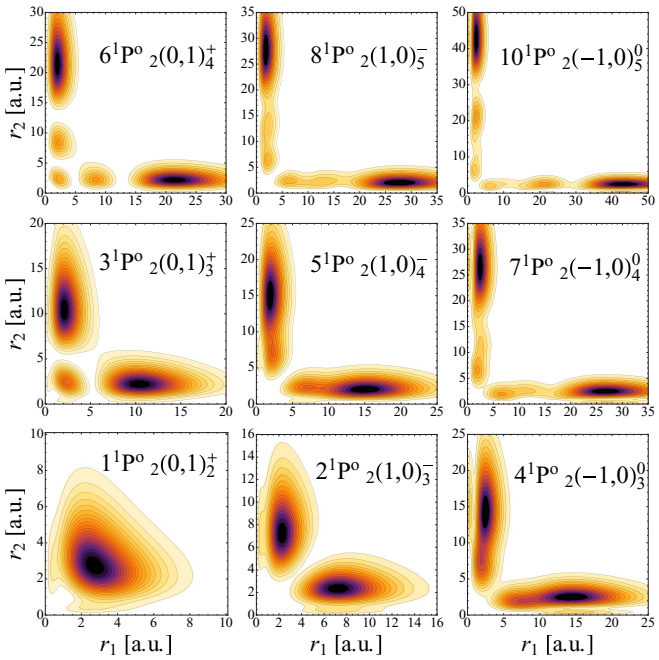

FIG. 1. (Color online) Two-electron radial density $\rho(r_1,r_2)r_1^2r_2^2$ for the lowest nine $^1P^o$ Feshbach resonance states in He, located below the second ionization threshold. Resonances are labeled according to the classification proposed by Lin [46] using $N\,{}^1P^o{}_{n_1}(K,T)^A_{n_2}$. Each column contains the three lowest resonances corresponding to a different $(K,T)^A$ series. The energy ordering indicated with the label N follows a zigzag pattern in the graphical array, according to the energies quoted in Table II. Inside each series, the increasing excitation energy is accompanied by an increasing number of radial nodes along r_1 (or r_2) for a given value of r_2 (r_1). Clearly the series with $A=-1$ shows a node in the bisection line $r_1=r_2$.

reasonable in terms of the general relation between energy and wave function compactness; the energy and entropy ordering coincide, except for the arrangement of states $[1sns,\,{}^1S^e;\ 1snp,\,{}^3P^o$; and $1snd,\,{}^1D^e]$ for low excitations $n=2$–5. For example, the pair $[S(1s2s,\,{}^1S^e)=5.492, S(1s2p,\,{}^3P^o)=5.356]$, or the triplet $[S(1s3s,\,{}^1S^e)=6.769,\ S(1s3p,\,{}^3P^o)=6.722,\ S(1s3d,\,{}^1D^e)=6.635]$ have opposite ordering for energies and entropies. Our results also show that an *entropic* first Hund's rule is satisfied, such that $S(1s2s,\,{}^3S^e)=5.236$ is below $S(1s2s,\,{}^1S^e)=5.492$, $S(1s2p,\,{}^3P^o)=5.356$ is less than $S(1s2p,\,{}^1P^o)=5.515$, $S(1s3s,\,{}^3S^e)=6.605$ lies below $S(1s3s,\,{}^1S^e)=6.769$, or $S(1s3d,\,{}^3D^e)=6.634$ is below $S(1s3d,\,{}^1D^e)=6.635$ (see Table I).

A similar analysis can be carried out with DES, whose Shannon entropies are included in Table II. The absence of the penetrating $1s$ orbital in their density structure makes the lowest Shannon entropy in DES be higher than the lowest one in the respective bound state of the same symmetry, $S[{}_2(1,0)^+_2,\,{}^1S^e]=6.380$ versus $S[1s^2,\,{}^1S^e]=2.705$. In the case of resonances, the entropic ordering also follows that of the energy within each (K,T) series at least for the lowest 6–7 resonances in each series. For DES it is not obvious to guess whether the first Hund's rule is satisfied or not, due to the strong mixing of hydrogen-like configurations within each (K,T) series. If one assumes for the $^{1,3}S^e$ DES a zeroth-order wave function (23), the energy difference between singlet and triplet comes from the different symmetrization in the participating $|2sn_2s\rangle$ and $|2pn_2p\rangle$ configurations, i.e., in the different values of the two-electron integrals for singlets and triplets. For example, by using Eq. (23) with $n_2=3$, a simple calculation gives -0.5656 a.u. for the singlet ${}_2(1,0)^+_3$ and -0.5921 a.u. for the triplet ${}_2(1,0)^-_3$. It also happens for higher members in the series with $n_2>3$. The same exercise carried out for the $(-1,0)$ series yields -0.4581 a.u. for the singlet ${}_2(-1,0)^+_3$ and -0.5193 a.u. for the triplet ${}_2(-1,0)^+_3$ and an analogous singlet-triplet ordering for higher n_2. In this way, the Hund's rule is satisfied (at least for the lowest calculated members) within the series $[{}_2(\pm1,0)^{+,-}_{n_2},\,{}^{1,3}S^e]$.

This behavior is indeed quite general in DES, with the exception of the series ${}_2(1,0)_{n_2}$ in the $^{1,3}P^o$ symmetries. In fact, by using now the DESB expression (24) for $n_2=3$ we find an opposite singlet-triplet energy ordering for the states ${}_2(1,0)_3$. We obtain -0.5824 a.u. for the singlet $[{}_2(1,0)_3,\,{}^1P^o]$ and -0.5535 a.u. for the triplet $[{}_2(1,0)_3,\,{}^3P^o]$, but -0.4708 a.u. for the singlet $[{}_2(-1,0)_3,\,{}^1P^o]$ and -0.5075 a.u. for the triplet $[{}_2(-1,0)_3,\,{}^3P^o]$, an energy ordering that agrees with the full CI results quoted in Table II. This is due to the combined effect of (i) the different values of the two-electron integrals for singlets and triplets and (ii) the presence of three mixing coefficients in Eq. (24), which change signs for the (1,0) and (0,1) series in such a way that the components of the energy corresponding to the crossed terms make the difference. In conclusion, although the individual IPM configurations in Eq. (24) always satisfy the Hund's rule, the combination does not. It is worth noting that using CI calculations we obtain the same entropic ordering even in this exceptional case $^1P^o$. For instance, $S[{}_2(1,0)^-_3,\,{}^1P^o]=7.970$ less than $S[{}_2(1,0)^+_3,\,{}^3P^o]=8.146$, with corresponding energies -0.597095 a.u. and -0.584929 a.u., and similarly for higher members with $n_2>3$.

Unfortunately, the Shannon entropy values hardly distinguish the evolution of the different DES ${}_2(K,T)_{n_2}$ series (within the same spectroscopic symmetry $^{2S+1}L^\pi$) along the increasing excitation in n_2. The S values for high-lying DES of any symmetry, spin, and (K,T) series overlap at extent within the same line, which eventually follows the direction of an asymptote located at the second ionization threshold $\mathrm{He}^+(n_1=2)$ with energy $E=-0.5$ a.u.

B. Fisher information

The Fisher information for singly excited states is shown in the left panels of Figs. 2 (singlets) and 3 (triplets). The behavior is notoriously different for each spectroscopic symmetry. In $^{1,3}S^e$ states the Fisher information decreases monotonically with the n_2 excitation. In contrast, the $^{1,3}P^o$ states increase monotonically their Fisher information with the excitation. Finally, in $^{1,3}D^e$ states it increases to reach a maximum, then decreases with higher excitation. Contrary to Shannon entropies, which should diverge at the first ionization threshold, the Fisher information reaches a constant value for all spectroscopic symmetries ($I[\rho]=8$ at energy $E=-2.0$ a.u.). This asymptotic value can be explained as follows. The spatial part of the wave function for highly excited states in the Rydberg series can be approximately

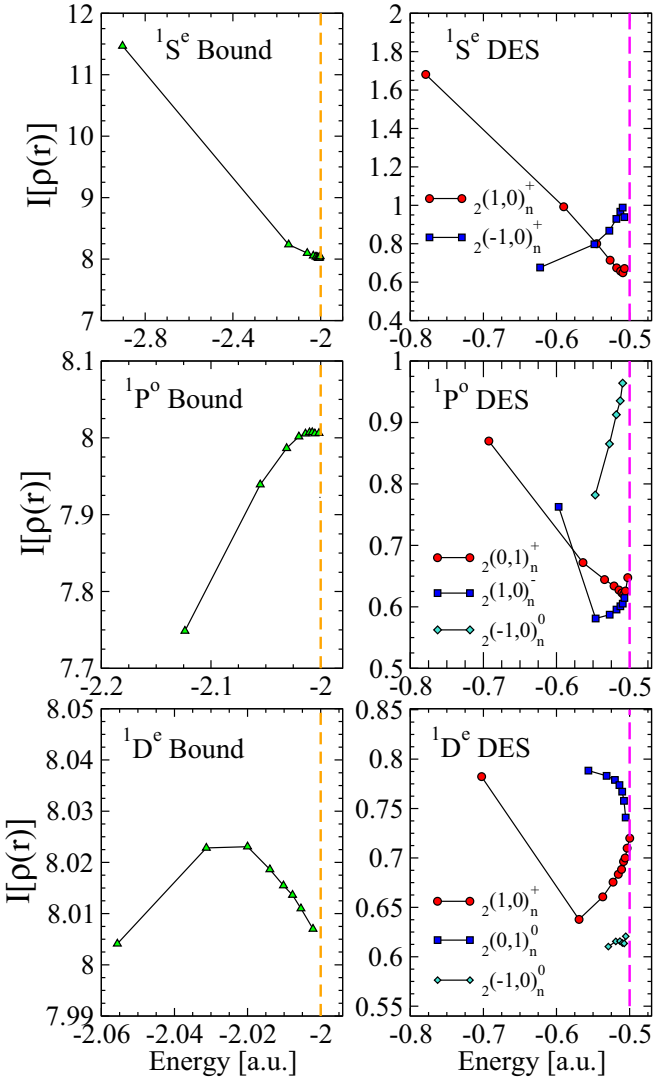

FIG. 2. (Color online) Fisher information $I[\rho(r)]$ for the ground state and the lowest members in the Rydberg series of singly excited $^1S^e$ states, singly excited $^1P^o$ states, and singly excited $^1D^e$ states in helium (left panel); and for the lowest members of the Rydberg series of doubly excited states organized according to series with different (K,T) labels: $^3S^e$ with two (K,T) series, $^3P^o$ with three series, and $^3D^e$ with three series (right panel). Solid lines connect points corresponding to states pertaining to the same Rydberg (K,T) series. Vertical dashed lines indicate the energy position for the thresholds He^+ $(n_1 = 1)$ (left panel) and He^+ $(n_1 = 2)$ (right panel).

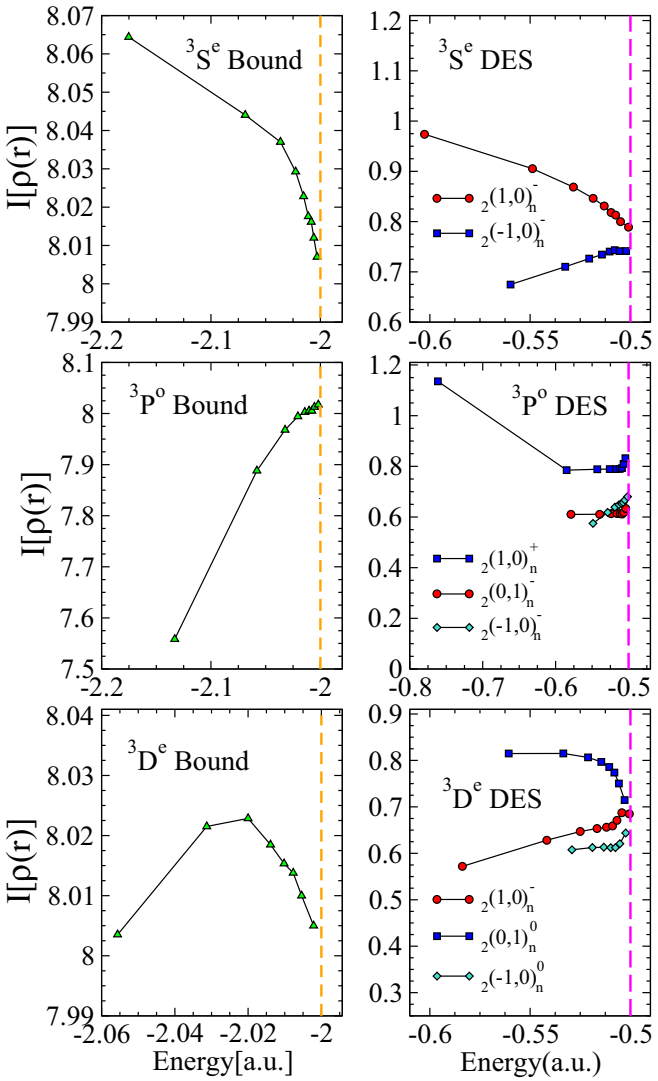

FIG. 3. (Color online) Same as Fig. 2 but for the spin triplets, for bound (left) and doubly excited states (right).

represented as a (anti)symmetrized product of a single IPM configuration where one of the electrons remains in the $1s$ orbital, i.e., $\Psi(r_1,r_2) = \frac{1}{\sqrt{2}}[\phi_{1s}(r_1)\phi_{n\ell}(r_2) \pm \phi_{n\ell}(r_1)\phi_{1s}(r_2)]$, whose reduced one-electron density is $\rho(r) = \frac{1}{2}[|\phi_{1s}(r)|^2 + |\phi_{n\ell}(r)|^2]$. With this density, the integrand of the Fisher information is

$$\frac{|\nabla\rho|^2}{\rho} = \frac{1}{2}\frac{|\nabla(|\phi_{1s}|^2)|^2}{[|\phi_{1s}|^2 + |\phi_{n\ell}|^2]} + \frac{1}{2}\frac{|\nabla(|\phi_{n\ell}|^2)|^2}{[|\phi_{1s}|^2 + |\phi_{n\ell}|^2]} + \frac{|\nabla(|\phi_{1s}|^2)||\nabla(|\phi_{n\ell}|^2)|}{[|\phi_{1s}|^2 + |\phi_{n\ell}|^2]}, \quad (25)$$

which can be approximated to give $I[\rho] \sim \frac{1}{2}I[1s]+\frac{1}{2}I[n\ell]$ plus a crossed term. Fortunately, the Fisher information for hydrogen-like densities is known exactly [67] to be $I[n\ell] = \frac{2Z^2}{n^3}\{n - \frac{2}{2\ell+1}[\ell(\ell+1)]\}$. When $n \to \infty$ both $I[n\ell]$ and the crossed term vanish, and the term containing the density of the residual target state $He^+(1s)$ remains, whose Fisher information value is 16. All singly excited states of any symmetry share the same target density at the first ionization threshold and therefore the same limit for the Fisher information.

Taking into account the exact values of the Fisher information for hydrogen-like atoms, the different tendencies of the Fisher information for the singly excited states can be also roughly explained. The $^1S^e$ ground state of He has the leading configuration $1s^2$ but also $1s2s$ may be considered. Similarly, the lowest $^1P^o$ state has a leading configuration $1s2p$ along with $1s3p$. Using the IPM wave functions for the configurations $1s^2$ and $1s2s$, their Fisher information is above 8, but for IPM configurations $1s2p$ and $1s3p$ their Fisher information is below 8, which is a combined effect

of (i) ns orbitals having higher Fisher information value than np orbitals and (ii) the higher value of the denominator $[|\phi_{1s}|^2+|\phi_{n\ell}|^2]$ in Eq. (25) for np than for ns orbitals. Also, the Fisher information function $I[n\ell]$ for hydrogen-like orbitals shows a maximum at $n_{max}=\frac{3\ell(\ell+1)}{2\ell+1}$ before tending to zero for $n\to\infty$. For instance, the d orbitals have a maximum in the Fisher information value for $n=4$. Similarly, this behavior also manifests in the singly excited states $1snd$ of symmetry $^{1,3}D^e$; the Fisher information reaches maximum values for the states $1s4d$ and $1s5d$. Slight deviations occur due to the CI mixing of excited configurations containing p,d,f,g, and h orbitals.

One might expect to use similar tools and reasoning to analyze the behavior of the Fisher information in DES of He, shown in the right panels of Figs. 2 and 3. These states also build a Rydberg series converging to the upper threshold limit $He^+(n_1=2)$, which in principle could intuitively impose two asymptotic values for the Fisher information, $I\sim\frac{1}{2}I(2s)=2$ and $I\sim\frac{1}{2}I(2p)=1/3$, in case that configurations for high-lying DES could also be written as IPM antisymmetrized configurations $2sns$ and $2pnp$ for $^{1,3}S^e$ (two Rydberg series), $2snp$, $2pns$, and $2pnd$ for $^{1,3}P^o$ (three series), and $2snd$, $2pnp$, and $2pnf$ for $^{1,3}D^e$ (three series). From our CI results plotted in Figs. 2 and 3, none of the Fisher information values for the calculated series of DES tend to 2 or 1/3 asymptotically. Thus the Fisher information represents a good indicator to confirm that DES are not well represented by simple IPM wave functions, at variance with single excitations.

Let us now assume that Rydberg series of DES are better represented by DESB states, according to Eq. (21), i.e., combinations of the Rydberg series of hydrogen-like IPM configurations. For instance, the two Rydberg series $(\pm1,0)$ of DESB states in $^{1,3}S^e$ states are given by the Eq. (23) and it is a simple exercise to calculate the Fisher information from this linear combination, although unfortunately one cannot arrive at a simple formula isolating each orbital contribution $I(2s)$ and $I(2p)$ to the Fisher information. If one makes the crude approximation $\rho(2s)=\rho(2p)$ and takes the limit $n_2\to\infty$ in the coefficients, one arrives at the approximate value $I\sim\frac{1}{4}(I[2s]+I[2p])=7/6$, thus indicating that the gross asymptotic limit is around unity. Without any approximation in using the density from Eq. (23) in Eq. (10), and varying n_2 (from 3 up to 60), we obtain a descending series with final value $I[_2(+1,0)_{60}]=0.7704$ and an ascending series with final value $I[_2(-1,0)_{60}]=0.7560$, values that seem to confirm our CI results for $^3S^e$ DES in Fig. 3. However, this prediction fails for the $^1S^e$ DES, a symmetry for which the two series cross to each other to finally reach different asymptotic limits (see Fig. 2). Similar analysis can be performed using Eq. (24) for the two $(\pm1,0)$ series and also, separately, for the $(0,1)$ series. We obtain for the three $(K,T)^A$ series in $^3P^o$ the following $(n_2=3\to n_2=60)$ correlations: $I[_2(+1,0)_3]=0.8678\to I[_2(+1,0)_{60}]=0.7714$ (decreasing with n_2), and $I[_2(-1,0)_3]=0.5859\to I[_2(-1,0)_{60}]=0.7532$ (increasing), and $I[_2(0,1)_3]=0.7211\to I[_2(0,1)_{60}]=0.6648$ (constant), which roughly follows the behavior of the *ab initio* results shown in Fig. 3. Again the predictions completely fail when applied to the singlets $^1P^o$. Another DESB formula for symmetry $^{1,3}D^e$ combines $|2snd\rangle$, $|2pnp\rangle$, and $|2pnf\rangle$ configurations. By using it for low $(n_2=3)$ and high excitations $(n_2=60)$ we obtain the Fisher information correlation values for $^{1,3}D^e$: $I[_2(+1,0)_3]=0.6305\to I[_2(+1,0)_{60}]=0.7707$ (increasing), $I[_2(-1,0)_3]=0.6907\to I[_2(-1,0)_{60}]=0.7536$ (increasing), and also $I[_2(0,1)_3]=0.8804\to I[_2(0,1)_{60}]=0.6619$ (decreasing). In $^{1,3}D^e$ our *ab initio* results in Figs. 2 and 3 have similar trends for singlets and triplets, but the above DESB predictions, in spite of giving roughly the tendencies, fail to give the highly excited asymptotic limits.

Surprisingly, in contrast to Shannon entropies, our *ab initio* calculations clearly indicate that the Fisher information is able to separate the trends of the different (K,T) series and to distinguish the different asymptotic values for each series at the second ionization threshold. These asymptotic values (not reducible to hydrogen-like contributions) are a signature of the intrinsic complexity of highly excited DES in helium, which exhibits such a strong configuration mixing that even a description in terms of intra- or intershell DESB states is not enough to fully explain the asymptotic values at threshold. In principle, it is a very remarkable result that the Fisher information of the single-electron density distribution be able to discriminate DES in terms of their local topological information provided by the gradient content, which brings us the conjecture that each (K,T) series of DES must be supported by a different family of quantum potentials $Q[\rho]=-\frac{\hbar^2}{2m}\frac{\nabla^2\sqrt{\rho}}{\sqrt{\rho}}$ *a la Bohm* in terms of the density, which can be extracted from the Fisher information since $I[\rho]=\frac{8m}{\hbar^2}\int d\mathbf{r}\rho Q[\rho]$ [51].

C. Entanglement measures: von Neumann and linear entropies

The von Neumann entropies of entanglement for the singlet and triplet bound, singly and doubly excited states in He are shown in Figs. 4 and 5. For the sake of comparison, we include in Table III our numerical results of linear and von Neumann entropies for the lowest $^{1,3}S^e$ states along with some existing data in previous works [29,30,38]. Linear entropies have also been calculated systematically, but we do not report the results (only those given in Table III).

In previous works [19,29,32,38] the von Neumann and linear entropies calculated only for bound states of symmetry

TABLE III. Linear and von Neumann entropies for the lowest bound $^{1,3}S^e$ states of helium compared to previous works [29,30,38].

	Ref. [29]	Ref. [30]		This work	
	S_L	S_L	S_{VN}	S_L	S_{VN}
$\|1s1s;^1S^e\rangle$	0.015914	0.01606	0.0785	0.0159306	0.078238
$\|1s2s;^1S^e\rangle$	0.48866	0.48871	0.991099	0.4887369	0.991153
$\|1s3s;^1S^e\rangle$	0.49857	0.49724	0.998513	0.4972512	0.998533
$\|1s4s;^1S^e\rangle$	0.49892	0.49892	0.999577	0.4989254	0.999588
$\|1s5s;^1S^e\rangle$	0.4993	0.499565	0.999838	0.4994713	0.999852
	Ref. [38]	Ref. [30]		This work	
$\|1s2s;^3S^e\rangle$	0.50038	0.500378	1.00494	0.5003759	1.004926
$\|1s3s;^3S^e\rangle$	0.50019	0.5000736	1.00114	0.5000732	1.001136
$\|1s4s;^3S^e\rangle$	0.49993	0.5000267	1.000453	0.5000265	1.000450
$\|1s5s;^3S^e\rangle$	0.50012	0.5000125	1.000091	0.5000125	1.000227

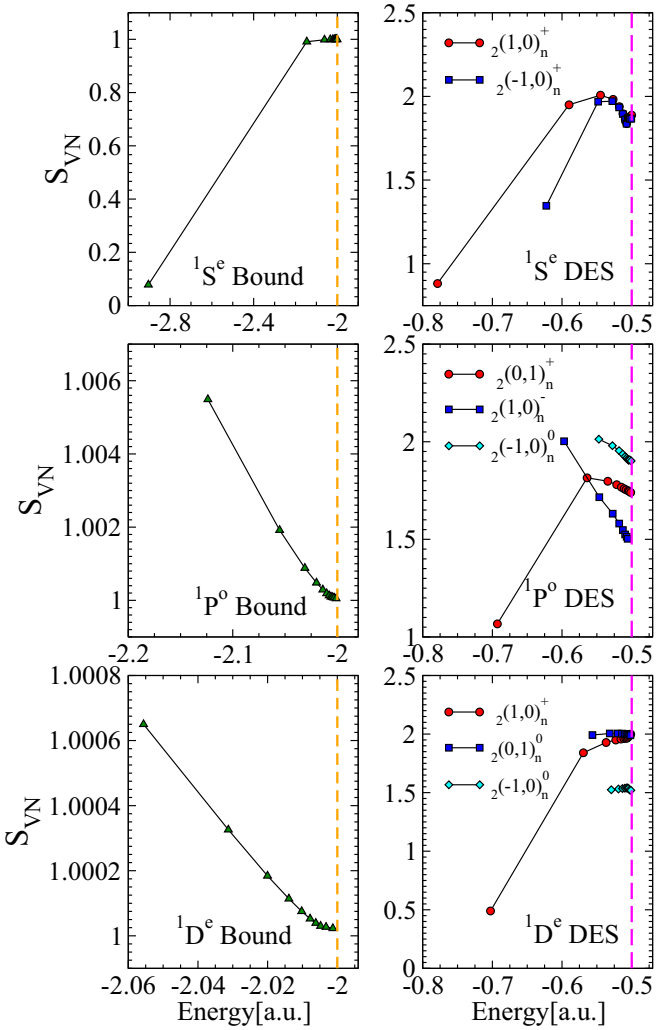

FIG. 4. (Color online) Von Neumann entropy S_{VN} for the ground state and the lowest members in the Rydberg series of singly excited ${}^1S^e$ states, singly excited ${}^1P^o$ states, and singly excited ${}^1D^e$ states in helium (left panel); and for the lowest members of the Rydberg series of doubly excited states organized according to series with different (K,T) labels: ${}^3S^e$ with two series, ${}^3P^o$ with three series, and ${}^3D^e$ with three series (right panel). Solid lines connect points corresponding to states pertaining to the same Rydberg (K,T) series. Vertical dashed lines indicate the energy position for the thresholds He^+ $(n_1 = 1)$ (left panel) and He^+ $(n_1 = 2)$ (right panel).

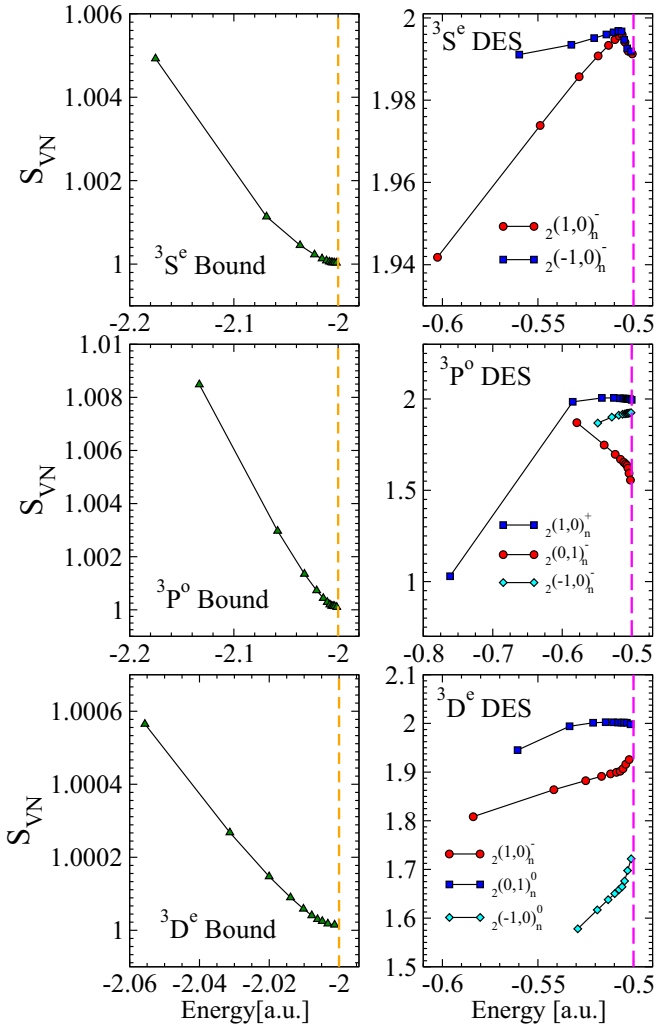

FIG. 5. (Color online) Same as Fig. 4 but for the spin triplets, for bound (left) and doubly excited states (right).

${}^1S^e$ led to the counterintuitive conclusion that entanglement increases monotonically with the excitation along the Rydberg series in agreement with general trends in model systems with non-Coulomb interactions [29]. This idea was subsequently amended after the calculation of the spin triplets ${}^3S^e$ in He [30,38]. In fact, from our systematic results for ${}^{1,3}S^e$, ${}^{1,3}P^o$, and ${}^{1,3}D^e$ we conclude that the bound ${}^1S^e$ states are the only exception to the opposite rule: the von Neumann and linear entropies always decrease monotonically with higher excitation, i.e., with the decreasing electron correlation and spatial separation between electrons in singly excited states.

The exceptional behavior of the entanglement entropies for ${}^1S^e$ bound states is related to the largest λ_1 eigenvalue from the set of eigenvalues $\{\lambda_i\}_{i=1}^M$ of the one-particle density matrix and to the form of the leading configurations in the CI expansion. The latter (equivalent or nonequivalent electron configurations) has an effect due to the form of the entanglement measure $\mathcal{E}_{VN}$ in Eq. (15) (see a brief discussion in Ref. [30]). For instance, our calculated ground state has $\lambda_1 = 0.9919$, and its CI coefficient $C_{1s1s} = 0.96187$ indicates a participation of 93% from the $(1s1s, {}^1S^e)$ configuration. The first eigenvalue λ_1 provides most of the von Neumann and linear entropy values, which are close to zero because the spatial wave function almost admits a representation in terms of a simple Hartree product of equivalent electrons that yields $\mathcal{E}_{VN} = S_{VN}[\hat{\rho}^{\text{spatial}}] = 0$. Since the dominant configuration for the ground state is that containing two equivalent electrons, its entanglement entropy approaches a zero value.

In contrast, for the first excited state $|1s2s, {}^1S^e\rangle$ the largest three λ's are $\lambda_1 = 0.5759$, $\lambda_2 = 0.4225$, and $\lambda_3 = 0.000252$, and the dominant configuration coefficients are $C_{1s2s} = -0.75532$ and $C_{1s3s} = 0.63465$. The first two values of λ already give $S_{VN} = 0.9830$ and $S_L = 0.4888$. Similar analysis can be performed for the rest of singly excited states, both singlets and triplets, for which none of the dominant configurations corresponds to two equivalent electrons. Now,

since both symmetric and antisymmetric two-electron spatial configurations $\frac{1}{\sqrt{2}}[\phi_{1s}(1)\phi_{n\ell}(2) \pm \phi_{n\ell}(1)\phi_{1s}(2)]$ (as well as two-electron spin configurations $\frac{1}{\sqrt{2}}[\alpha(1)\beta(2) \pm \beta(1)\alpha(2)]$) yield $S_{VN} = 1$, it is understood that as $n \to \infty$ along the Rydberg series $\mathcal{E}_{VN}$ reaches the asymptotic limit of unity for a noninteracting state, whose spatial von Neumann entropy value cancels due to antisymmetrization but the spin contribution remains according to Eq. (15). From the inspection of the left panels in Figs. 4 and 5, it is clear that all Rydberg series of singly excited states tend asymptotically to spin-entangled states as $n \to \infty$, to limiting values $S_{VN} = 1$ (and $S_L = 0.5$ for linear entropies), associated with the first ionization threshold $\mathrm{He}^+(1s)$. Also, in bound states of He, the exact asymptotic ratio $S_{VN}/S_L = 2$ for $n \to \infty$ shows slight deviations at lower energies (except for the ground state) due to the neglected high-order contributions when expanding $\log_2 \hat{\rho}$ in the von Neumann entropy to obtain the linear entropy.

The most interesting results obtained in this section correspond to the entanglement measures obtained for DES in He. Here we only comment on the von Neumann entropy results, since linear entropy values are qualitatively similar and they are almost parallel to the von Neumann entropy curves. In fact, only those lowest lying DES that are closer to a single configuration representation (for instance, $[_2(1,0)_2^+, {}^1S^e]$, $[_2(0,1)_2^+, {}^1P^o]$, or $[_2(1,0)_2^+, {}^3P^o]$ with $S_{VN} \sim 1$) have a ratio $S_{VN}/S_L \sim 2$, but for higher excitations with increasing n_2 in DES the ratio S_{VN}/S_L is around 2.7.

Our results show three main characteristics:

(1) von Neumann entropies of DES may increase or decrease monotonically with the excitation according to their classification to a given (K,T) series, but eventually they may also exhibit maxima before reaching their asymptotic value at the second ionization threshold;

(2) von Neumann entropies of DES tend to a plethora of different asymptotic limits at the second ionization threshold which depend upon the (K,T) labels and the total symmetry ${}^{2S+1}L^{\pi}$;

(3) all asymptotic values of von Neumann entropies at the second ionization threshold $\mathrm{He}^+(n_1 = 2)$ are larger than unity (the constant spin contribution to entanglement), which can be interpreted as a remnant entanglement accompanying high excitation in DES.

As mentioned above, some series such as $(\pm 1,0)\ {}^{1,3}S^e$ and $(0,1)\ {}^1P^o$ show a maximum before decreasing to their limiting value. The same (K,T) series may show a completely different behavior in singlets and triplets. For instance, $(\pm 1,0)$ and $(0,1)$ series behave differently in ${}^1P^o$ and ${}^3P^o$, or in ${}^1D^e$ and ${}^3D^e$, when, in principle, no such singlet-triplet distinction is inferred from Eq. (21) [see also Eq. (24)].

The lowest DES $[_2(1,0)_2^+, {}^1S^e]$ has a low entropy value below unity, $S_{VN} = 0.882$, for reasons similar to those explained for the ground state $1s^2\ {}^1S^e$. For this DES there are two dominant eigenvalues of the reduced density matrix $\lambda_1 = 0.71729$ and $\lambda_2 = 0.28041$ with the rest close to zero, and the dominant CI coefficients are $C_{2s2s} = 0.83114$ and $C_{2p2p} = 0.49602$, which indicates that this DES is mostly described as a combination of *two* configurations with equivalent electrons, instead of one. By just extracting the latter expansion coefficients from the CI wave function, the *unnormalized* reduced density matrix is already diagonal in the basis of orbitals $\{2s,2p\}$ with eigenvalues $C^2_{2s2s} = 0.6908$ and $C^2_{2p2p} = 0.2460$, close to the *ab initio* ones and an approximate entropy value $S_{VN} = 0.866$, also below unity. This is in accord with the expansion coefficients $(3/4)^{1/2}$ and $(1/4)^{1/2}$ for (1,0) DESB states in Eq. (23) when $n_2 = 2$, which produce eigenvalues $\lambda_1 = 0.75$ and $\lambda_2 = 0.25$ and an entropy value $S_{VN} = 0.811$.

The second lowest DES $[_2(-1,0)_2^+, {}^1S^e]$ has $S_{VN} = 1.346$, with *ab initio* dominant eigenvalues $\lambda_1 = 0.62116$ and $\lambda_2 = 0.30782$ and expansion coefficients $C_{2s2s} = 0.42989$ and $C_{2p2p} = -0.70541$. Again, by only using these coefficients to construct a 2×2 reduced density matrix, the diagonal elements are 0.1848 and 0.4976, from which one obtains $S_{VN} = 0.951$, larger than for the lowest ${}^1S^e$ DES but below the *ab initio* result. Here, Eq. (23) provides the same density matrix for $(\pm 1,0)$ and thus the same entropy value, $S_{VN} = 0.811$. Separately, we can diagonalize the 2×2 Hamiltonian in the DESB manifold $\{2s^2, 2p^2\}$, producing two energy eigenvalues -0.7540 and -0.5116 with expansion coefficients $C_{2s2s} = 0.87972$ and $C_{2p2p} = 0.47548$ for the lowest DES and $C_{2s2s} = 0.47548$ and $C_{2p2p} = -0.87972$ for the second lowest one. These values are close to (but not the same as) the coefficients of DESB states $(3/4)^{1/2}$ and $(1/4)^{1/2}$ in Eq. (23). The corresponding von Neumann entropy obtained from the two eigenstates of this 2×2 Hamiltonian is the same for both states, $S_{VN} = 0.770$, below the value $S_{VN} = 0.811$ obtained from the DESB mixture. In conclusion, in contrast to the lowest DES, the second lowest DES $[_2(-1,0)_2^+, {}^1S^e]$ requires more than two configurations to describe its correlations and entanglement. This tendency to mix more configurations increases with higher excitation in DES.

${}^{1,3}S^e$ DES have a common asymptotic entropy $S_{VN} \sim 2$. This limit seems to be explained from the DESB states in Eq. (23). The associated 4×4 reduced density matrix has two degenerated eigenvalues $\{2 \times \frac{n_2+1}{4n_2}, 2 \times \frac{n_2-1}{4n_2}\}$ and from them

$$S_{VN}^{(\pm 1,0)}[n_2] = -\log_2 \frac{(n_2+1)^{\frac{n_2+1}{2n_2}}(n_2-1)^{\frac{n_2-1}{2n_2}}}{4n_2}, \qquad (26)$$

an expression that fails to compare with *ab initio* results for low values of n_2, but its limit for $n_2 \to \infty$ is exactly 2.

In order to unveil the trends of the von Neumann entropy in our full CI calculations, we keep on analyzing results in ${}^1P^o$ DES by reducing the configurational space to only those intra- and intershell configurations that enter in the DESB states in Eq. (24). The lowest DES with label $[_2(0,1)_2^+, {}^1P^o]$ is special, because in the corresponding DESB expression only the $2s2p$ configuration participates. Since this DES is thus described at lowest order by a single antisymmetrized IPM configuration, its von Neumann entropy value must be closer to unity. The same happens to occur with the lowest DES in ${}^3P^o$, $[_2(1,0)_2^+, {}^3P^o]$ (see Fig. 5), and the lowest DES in ${}^1D^e$, $[_2(1,0)_2^+, {}^1D^e]$ (Fig. 4). From $n_2 = 2$ to $n_2 = 3$ there is a sudden jump to a higher entropy value because for $n_2 \geqslant 3$, the three intershell configurations in the DESB manifold participate. For example, in the ${}^{1,3}P^o$ symmetry for the $(\pm 1,0)$ series, DESB states are built up with the configurational manifold $\{2sn_2p, 2pn_2s, 2pn_2d\}$ from $n_2 = 3$ to $n_2 \to \infty$. We can proceed by building up the 5×5 reduced density matrix with two approaches: first, using the DESB expansion coefficients;

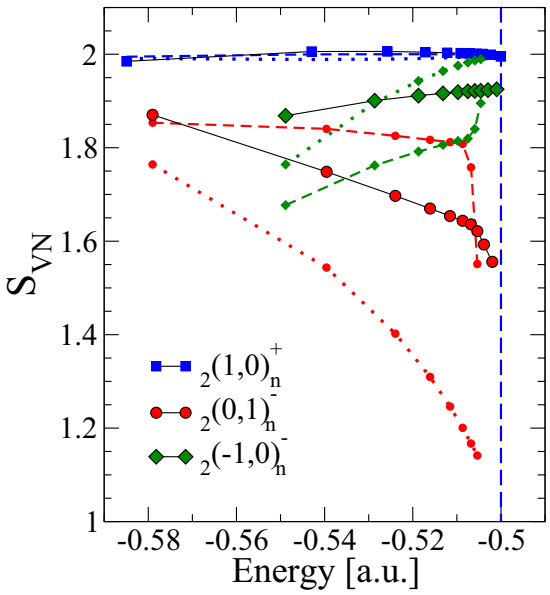

FIG. 6. (Color online) Von Neumann entropy S_{VN} for the lowest members in the Rydberg series of $^3P^o$ DES; blue squares for the (1,0) series, red circles for the (0,1) series, and green diamonds for (−1,0). Solid line: full CI *ab initio* results; dashed line: 3 × 3 Hamiltonian results from Eq. (27) and $Z \to \infty$; dotted line: results from the DESB combinations using Eqs. (28) and (29). The von Neumann entropy values from the three different approaches are set up with the same *ab initio* DES energies for the sake of comparison. The vertical dashed line indicates the energy position for the threshold $He^+(n_1 = 2)$.

second, using the coefficients from the 3 × 3 Hamiltonian eigenstates. The Hamiltonian matrix for a helium-like atom with nuclear charge Z has the form

$$H = -\frac{Z^2}{2}\left[\frac{1}{2^2}+\frac{1}{n_2^2}\right]\begin{pmatrix}1&0&0\\0&1&0\\0&0&1\end{pmatrix} + Z\begin{pmatrix}\langle 2sn_2p|2sn_2p\rangle & \langle 2sn_2p|2pn_2s\rangle & \langle 2sn_2p|2pn_2d\rangle\\ \langle 2pn_2s|2sn_2p\rangle & \langle 2pn_2s|2pn_2s\rangle & \langle 2pn_2s|2pn_2d\rangle\\ \langle 2pn_2d|2sn_2p\rangle & \langle 2pn_2d|2pn_2s\rangle & \langle 2pn_2d|2pn_2d\rangle\end{pmatrix}, \tag{27}$$

and the only required input values are the two-electron integrals computed for $Z = 1$, for a given excitation n_2 and a given spin symmetry.

With the first approach, building the reduced density matrix from the DESB expansion coefficients for $^{1,3}P^o$ states, one obtains four eigenvalues for the (±1,0) series, from which the von Neumann entropy has the analytical expression

$$S_{VN}^{(\pm1,0)}[n_2] = -\log_2\left[\frac{1}{4n_2^2}\left(n_2^2 \pm n_2 - 2\right)^{\frac{n_2^2\pm n_2-2}{2n_2^2}} \times \left(n_2^2 \mp n_2 + 2\right)^{\frac{n_2^2\mp n_2+2}{2n_2^2}}\right]. \tag{28}$$

This formula for the (+1,0) series produces a function of n_2 almost constant with an asymptotic limit 2 (see Fig. 6). The series (−1,0) starts at $S_{VN}^{(-1,0)}[n_2 = 3] = 1.764$, then it increases monotonically to also reach the limit 2. Finally, the von Neumann entropy for the (0,1) series has the expression

$$S_{VN}^{(0,1)}[n_2] = -\log_2\left[\frac{1}{n_2^2}\left(\frac{n_2^2-2}{2}\right)^{1-2/n_2^2}\right], \tag{29}$$

from which $S_{VN}^{(0,1)}[n_2 = 3] = 1.764$ and rapidly decreases to reach its asymptotic value equal to unity as shown in Fig. 6. Also, in Fig. 6 we have included for comparison the entropy values obtained from the reduced 3 × 3 Hamiltonian, calculated for the $^3P^o$ symmetry and taking $Z \to \infty$ in Eq. (27) (the noninteracting limit for highly charged ions), because this case produces the best comparison between DESB formulas and the reduced Hamiltonian [44]. This comparison in $^3P^o$ between the *ab initio* results and those extracted from these DESB simplified models indicates that whereas the increasing or decreasing trends of the different (K,T) series is roughly explained, the asymptotic limits for high excitation are not always correctly reproduced. For worse, predictions from both DESB states and the 3 × 3 model Hamiltonian dramatically fail to explain the *ab initio* results for the singlets $^1P^o$, and also for $^{1,3}D^e$ DES [where (K,T) series are sharply separated], thus precluding a simple analysis on these complex DES.

IV. CONCLUSIONS AND PERSPECTIVES

In this work we have systematically analyzed bound and doubly excited states in the spectroscopic symmetries $^{1,3}L^{e,o}$ $(L = 0,1,2)$ from the perspective of information-theoretic measures based on the reduced one-particle spatial density $\rho(r)$ (Shannon entropies and Fisher information) as well as on the reduced one-particle density matrix $\hat{\rho}$ (entanglement measures). Our results on Shannon entropies show that this global measure operated over the one-particle density always increases monotonically with excitation for both singly and doubly excited states in He (as expected from the increasing spatial spreading of the wave function with excitation) but it is not able to discriminate double excited states as pertaining to different $(K,T)^A$ series. However, we find that Shannon entropies are sensitive enough to manifest a close relationship between the energy ordering and the Shannon-entropy values for states in He. In this respect, we find that a *Shannon-entropic* first Hund's rule is satisfied to some extent.

In relation to the gradient content given by the Fisher information, we find for singly excited states that it behaves differently according to the total angular symmetry L: it decreases monotonically for $^{1,3}S^e$ singly excited states, it increases monotonically for $^{1,3}P^o$ states, and it shows maxima for $^{1,3}D^e$ states. Every singly excited state in He reaches the high-excitation asymptotic limit $I[\rho(r)] = 8$ corresponding to the parent ion state $He^+(1s)$. In contrast, for DES, we find a variety of increasing and decreasing tendencies of the Fisher information against the excitation for the different (K,T) series within the same total angular symmetry L, without encompassing a general rule. Whereas those Rydberg asymptotic values of Fisher information at the first ionization threshold $He^+(1s)$ can be established for singly excited states without ambiguity, to locate and explain the variety of limits at the second ionization threshold $He^+(2s,2p)$ is much more involved, even by using the approximate description in terms

of DESB. In spite of this, it is quite a surprising and notable result that the Fisher information is helpful to also classify DES as pertaining to different $(K,T)^A$ series, thus revealing itself as a tool to partially disclose the inherent complexity of DES. This unexpected capability of the Fisher information to discriminate DES in $(K,T)^A$ series as entanglement measures also do may indicate a possible connection between these in principle unrelated entities, yet unknown.

Contrary to some previously established ideas derived from studies in model systems, we find that within bound states in He below the first ionization threshold, the entropies of entanglement decrease with the excitation as a regular rule, which is intuitively expected in terms of the ensuing decreasing electron correlation and the increasing spatial separation among electrons. The symmetry $^1S^e$ is the only exception due to the dominant equivalent electron character in the wave function of the ground state and to the entanglement definition that treats on equal footing equivalent and nonequivalent spatial electron configurations sharing the same spin wave function. Highly singly excited states reach the asymptotic limit $S_{VN} = 1$ ($S_L = 0.5$), which corresponds solely to the spin contribution to entanglement since the spatial wave function, which reduces to a single antisymmetrized IPM configuration $(1s,n\ell)$ for $n \gg 1$, does not contribute to entanglement according to the measure used. Similarly to the Fisher information, the entanglement values of DES can be better rationalized in terms of the different tendencies shown by the members associated with a given $(K,T)^A$ series, which nevertheless show a profusion of increasing and decreasing trends against the excitation energy (which breaks down our previous intuition gained in singly excited states on the relation between entanglement, electron repulsion, and spatial separation). Also, a limiting value of entanglement (especially in S and P DES) is discriminated for each $(K,T)^A$ series at the second ionization threshold $He^+(2s,2p)$, a value which is hardly explained even with a detailed analysis in terms of approximate DESB states.

These resonant states in He become a realistic paradigmatic example of complexity in revealing their essential entanglement, even in the noninteracting limit due to the intrinsic degeneracy of intra- and intershell configurations entering in the low-order approximate description through DESB states. In other words, the $1/r_{12}$ electron correlation interaction mixes IPM configurations in the DESB description of DES, even when the nuclear charge $Z \to \infty$, or simply by using $1/r_{12}$ as a perturbation in degenerate perturbation theory [13,21]. A more accurate *ab initio* description of DES using the CI method brings additional correlations by including many other intra- and intershell configurations, resulting in a different remnant entanglement (on top of the constant spin contribution) for each (K,T) series of DES for almost any high excitation up to the second ionization threshold $He^+(n = 2)$, in contrast to the clear-cut limits of entanglement in singly excited states of He.

Whereas radial correlations vary with the nuclear charge Z, angular correlations (ℓ_1,ℓ_2) or (K,T) are almost constant along the isoelectronic series. Plots of DES energies against $1/Z$ show a plethora of avoided crossings for low values of Z (especially around $Z = 2$ for He) which precludes simple and successful classification schemes in strongly correlated atoms [44]. Instead, in the $Z \to \infty$ limit, DES wave functions are known to behave closer to an intrashell DESB basis. This means that in this work we have chosen indeed the most involved case from the helium isoelectronic series, for which our full *ab initio* results, although partially interpreted with the aid of DESB states, cannot be reduced in terms of them.

It was established [46] that DES with identical $(K,T)^A$ but different spectroscopic L, S, and π symmetries have isomorphic electron correlations since they have similar channel potential curves in hyperspherical coordinates. According to this, for example, the $(1,0)^+$ state is present in the symmetries $^1S^e$, $^3P^o$, and $^1D^e$, and the $(-1,0)^-$ state appears in the $^3S^e$, $^1P^o$, and $^3D^e$ symmetries, and the $(-1,0)^0$ state is in the $^1P^o$, $^1D^e$, and $^3D^e$ symmetries. In principle, one may expect similar values for the entities calculated in this work for these isomorphic $(K,T)^A$ series, but these similarities are not present in the Fisher information or in the entanglement measures whatsoever.

Extensions of this work to alkaline-earth atoms is feasible [54], assuming they behave as systems with outer-shell two-active electrons with a core interaction. The role of a polarizable core is not only that of a simple screening, but it also has an effect on the different combinations that generate their particular DESB states. Only for two-electron atoms the total wave function can be separated in its spatial and its spin part, which allows for a separate calculation of the spin contribution to the entanglement, being a constant value. This separability cannot be extended to atoms with three or more electrons, which means than the entanglement must be considered as a whole spatial-spin entity. Three-electron atomic systems have already been studied in our group with CI methods, using hydrogen-like orbitals [60,68], Hylleraas-type bases [69], and Slater-type orbitals [61], which open to us the possibility to extend these theoretic-information studies beyond the two-fermion case in atoms.

ACKNOWLEDGMENTS

We acknowledge financial support by Universidad de Antioquia (Vicerrectoría de Investigación CODI Mediana Cuantía project E01538 and Estrategia de Sostenibilidad 2013-2014). J.P.R.C. acknowledges AUIP (Asociación Universitaria Iberoamericana de Posgrados) for partial financial support granted to cover a half-semester stay at Universidad de Granada. We also thank Juan Carlos Angulo (Universidad de Granada) for helpful discussions and for his kind hospitality extended to both authors.

[1] K. D. Sen, J. Chem. Phys. **123**, 074110 (2005).
[2] A. Nagy, Chem. Phys. Lett. **425**, 154 (2006).
[3] K. D. Sen, J. Antolín, and J. C. Angulo, Phys. Rev. A **76**, 032502 (2007).
[4] J. C. Angulo, J. Antolín, and K. D. Sen, Phys. Lett. A **372**, 670 (2008).
[5] J. C. Angulo, J. Antolín, S. López-Rosa, and R. O. Esquivel, Physica A **389**, 899 (2010).

[6] C. Amovilli and N. H. March, Phys. Rev. A **69**, 054302 (2004).
[7] Q. Shi and S. Kais, Chem. Phys. **309**, 127 (2005).
[8] E. Romera, P. Sánchez-Moreno, and J. S. Dehesa, Chem. Phys. Lett. **414**, 468 (2005).
[9] J. S. Dehesa, S. López-Rosa, B. Olmos, and R. J. Yáñez, J. Comput. Appl. Math. **179**, 185 (2005).
[10] L. Amico, R. Fazio, A. Osterloh, and V. Vedral, Rev. Mod. Phys. **80**, 517 (2008).
[11] A. R. Plastino, D. Manzano, and J. S. Dehesa, Europhys. Lett. **86**, 20005 (2009).
[12] R. Horodecki, P. Horodecki, M. Horodecki, and K. Horodecki, Rev. Mod. Phys. **81**, 865 (2009).
[13] M. C. Tichy, F. Mintert, and A. Buchleitner, J. Phys. B: At., Mol. Opt. Phys. **44**, 192001 (2011).
[14] F. Carlier, A. Mandilara, and A. Sarfati, J. Phys. B: At., Mol. Opt. Phys. **40**, S199 (2007).
[15] J. Pipek and I. Nagy, Phys. Rev. A **79**, 052501 (2009).
[16] A. Ferrón, O. Osenda, and P. Serra, Phys. Rev. A **79**, 032509 (2009).
[17] F. M. Pont, O. Osenda, J. H. Toloza, and P. Serra, Phys. Rev. A **81**, 042518 (2010).
[18] R. J. Yáñez, A. R. Plastino, and J. S. Dehesa, Eur. Phys. J. D **56**, 141 (2010).
[19] D. Manzano, A. R. Plastino, J. S. Dehesa, and T. Koga, J. Phys. A: Math. Theor. **43**, 275301 (2010).
[20] P. A. Bouvrie, A. P. Majtey, A. R. Plastino, P. Sánchez-Moreno, and J. S. Dehesa, Eur. Phys. J. D **66**, 15 (2012).
[21] A. P. Majtey, A. R. Plastino, and J. S. Dehesa, J. Phys. A: Math. Theor. **45**, 115309 (2012).
[22] P. Kościk, Phys. Lett. A **377**, 2393 (2013).
[23] Z. Huang, H. Wang, and S. Kais, J. Mod. Opt. **53**, 2543 (2006).
[24] O. Osenda and P. Serra, Phys. Rev. A **75**, 042331 (2007).
[25] J. P. Coe, A. Sudbery, and I. D'Amico, Phys. Rev. B **77**, 205122 (2008).
[26] I. A. Howard, K. D. Sen, A. Borgoo, and P. Geerlings, Phys. Lett. A **372**, 6321 (2008).
[27] I. A. Howard, A. Borgoo, P. Geerlings, and K. Sen, Phys. Lett. A **373**, 3277 (2009).
[28] J. P. Coe and I. D'Amico, J. Phys.: Conf. Ser. **254**, 012010 (2010).
[29] J. S. Dehesa, T. Koga, R. J. Yáñez, A. R. Plastino, and R. O. Esquivel, J. Phys. B: At., Mol. Opt. Phys. **45**, 015504 (2012).
[30] G. Benenti, S. Siccardi, and G. Strini, Eur. Phys. J. D **67**, 83 (2013).
[31] T. S. Hofer, Front. Chem. **1**, 24 (2013).
[32] Y.-C. Lin, C.-Y. Lin, and Y. K. Ho, Phys. Rev. A **87**, 022316 (2013).
[33] C.-H. Lin, Y.-C. Lin, and Y. K. Ho, Few-Body Syst. **54**, 2147 (2013).
[34] G. C. Ghirardi and L. Marinatto, Phys. Rev. A **70**, 012109 (2004).
[35] G. C. Ghirardi and L. Marinatto, Fortschr. Phys. **52**, 1045 (2004).
[36] F. Buscemi, P. Bordone, and A. Bertoni, Phys. Rev. A **75**, 032301 (2007).
[37] O. Osenda and P. Serra, J. Phys. B: At., Mol. Opt. Phys. **41**, 065502 (2008).
[38] J. S. Dehesa, T. Koga, R. J. Yáñez, A. R. Plastino, and R. O. Esquivel, J. Phys. B: At., Mol. Opt. Phys. **45**, 239501 (2012).
[39] U. Fano, Phys. Rev. **124**, 1866 (1961).
[40] J. W. Cooper, U. Fano, and F. Prats, Phys. Rev. Lett. **10**, 518 (1963).
[41] D. R. Herrick and O. Sinanoğlu, Phys. Rev. A **11**, 97 (1975).
[42] C. D. Lin, Phys. Rev. A **29**, 1019 (1984).
[43] G. S. Ezra and R. S. Berry, Phys. Rev. A **28**, 1974 (1983).
[44] A. Macías and A. Riera, Phys. Rev. A **40**, 4298 (1989).
[45] D. R. Herrick, in *Advances in Chemical Physics*, edited by I. Prigogine and S. A. Rice, Vol. 52 (John Wiley & Sons, Inc., Hoboken, NJ, 1982).
[46] C. D. Lin, Phys. Rev. Lett. **51**, 1348 (1983).
[47] C. M. Granados-Castro and J. L. Sanz-Vicario, J. Phys. B: At., Mol. Opt. Phys. **46**, 055601 (2013).
[48] D. G. Ellis, Phys. Rev. A **53**, 3986 (1996).
[49] C. F. von Weizsäcker, Z. Phys. **96**, 431 (1935).
[50] D. Bohm, Phys. Rev. **85**, 166 (1952).
[51] M. Reginatto, Phys. Rev. A **58**, 1775 (1998).
[52] J. Schliemann, J. I. Cirac, M. Kuś, M. Lewenstein, and D. Loss, Phys. Rev. A **64**, 022303 (2001).
[53] J. Naudts and T. Verhulst, Phys. Rev. A **75**, 062104 (2007).
[54] J. C. Cardona and J. L. Sanz-Vicario, J. Phys. B: At., Mol. Opt. Phys. **41**, 055003 (2008).
[55] R. McWeeny, *Methods of Molecular Quantum Mechanics* (Academic Press, New York, 1992).
[56] A. U. Hazi and H. S. Taylor, Phys. Rev. A **1**, 1109 (1970).
[57] W. P. Reinhardt, Annu. Rev. Phys. Chem. **33**, 223 (1982).
[58] H. Feshbach, Ann. Phys. (NY) **19**, 287 (1962).
[59] H. Friedrich, *Theoretical Atomic Physics* (Springer-Verlag, Heidelberg, 1991).
[60] J. L. Sanz-Vicario, J. C. Cardona, and E. Lindroth, Phys. Rev. A **78**, 053411 (2008).
[61] J. C. Cardona, J. L. Sanz-Vicario, and F. Martín, Phys. Rev. A **82**, 022501 (2010).
[62] A. F. Ordóñez-Lasso, J. C. Cardona, and J. L. Sanz-Vicario, Phys. Rev. A **88**, 012702 (2013).
[63] M. K. Chen, Phys. Rev. A **56**, 4537 (1997).
[64] M. Cortés, A. Macías, F. Martín, and A. Riera, J. Phys. B: At., Mol. Opt. Phys. **26**, 3269 (1993).
[65] F. A. de Saavedra, I. Porras, E. Buendía, and F. J. Gálvez, J. Phys. B: At., Mol. Opt. Phys. **28**, 3123 (1995).
[66] R. J. Yáñez, W. Van Assche, and J. S. Dehesa, Phys. Rev. A **50**, 3065 (1994).
[67] J. S. Dehesa, S. López-Rosa, B. Olmos, and R. J. Yáñez, J. Math. Phys. **47**, 052104 (2006).
[68] J. L. Sanz-Vicario, E. Lindroth, and N. Brandefelt, Phys. Rev. A **66**, 052713 (2002).
[69] J. C. Cardona, Ph.D. thesis, Universidad de Antioquia, Medellín, Colombia, 2008.